Rapid Near-Optimal Trajectory Generation and Guidance Law Development for Single-Stage-to-Orbit Airbreathing Vehicles

January 1990

Research Supported by
NASA Langley Research Center

NASA Contract Number NAG-1-922

FINAL Technical Report

Principal Investigators: A. J. Calise and G. A. Flandro
Research Assistant: J. E. Corban
NASA Contract Monitor: D. D. Moerder

School of Aerospace Engineering
Georgia Institute of Technology
Atlanta, Georgia 30332

Rapid Near-Optimal Trajectory Generation and Guidance Law Development for Single-Stage-to-Orbit Airbreathing Vehicles

January 1990

Research Supported by
NASA Langley Research Center

NASA Contract Number NAG-1-922

Principal Investigators: A. J. Calise and G. A. Flandro
Research Assistant: J. E. Corban
NASA Contract Monitor: D. D. Moerder

School of Aerospace Engineering
Georgia Institute of Technology
Atlanta, Georgia 30332

Summary

During the current reporting period, January 1 to December 31, 1989, general problems associated with on-board trajectory optimization, propulsion system cycle selection, and with the synthesis of guidance laws were addressed for ascent to low-Earth-orbit of an air-breathing, single-stage-to-orbit vehicle. This report follows a previous one entitled "Trajectory Optimization and Guidance Law Development for National Aerospace Plane Applications" and dated December 1988. The work reported herein builds directly upon the analytical results presented in that document. A good portion of this work focused on making improvements to the vehicle models employed. The NASA "Generic Hypersonic Aerodynamic Model Example" and the "Langley Accelerator" aerodynamic data sets were acquired and implemented. Work pertaining to the development of purely analytic aerodynamic models also continued at a low level. A generic model of a multi-mode propulsion system was developed that includes turbojet, ramjet, scramjet, and rocket engine cycles. Provisions were made in the dynamic model for a component of thrust normal to the flight path. Computational results, which characterize the nonlinear sensitivity of scramjet performance to changes in vehicle angle of attack, were obtained and incorporated into the engine model. Additional trajectory constraints were also introduced. The constraints now treated are: maximum dynamic pressure, maximum aerodynamic heating rate per unit area, angle of attack and lift limits, and limits on acceleration both along and normal to the flight path.

The remainder of the research effort focused, for the most part, on required modifications to the previously derived algorithm when the model complexity cited above was added. In particular, analytic switching conditions were derived which, under appropriate assumptions, govern optimal transition from one propulsion mode to another for two cases: the case in which engine cycle operations can overlap, and the case in which engine cycle operations are mutually exclusive. The resulting guidance algorithm was implemented in software and exercised extensively. It was found that the approximations associated with the assumed time scale separation employed in this work are reasonable except over the Mach range from roughly 5 to 8. This phenomenon is due to the very large thrust capability of scramjets in this Mach regime when sized to meet the requirement for ascent to orbit. Very little mass penalty is induced by the resulting inaccuracies in the trajectory over this region because it is traversed rapidly. However, the reduced solution climb paths prove to be unfeasible within this Mach range when subject to the full model dynamics and active trajectory constraints. These difficulties were successfully overcome by accounting for flight path angle and flight path angle rate in construction of the flight path over this Mach range. The resulting algorithm provides the means for rapid near-optimal trajectory generation and propulsion cycle

selection over the entire Mach range from take-off to orbit given a realistic nonlinear vehicle model and all pertinent trajectory constraints.

The only significant problem area encountered to date relates to the lack of a general theory for singularly perturbed systems that are subject to state-variable inequality constraints. Such constraints are common to a wide class of flight vehicles but have received little attention in the literature when the dynamic system is singularly perturbed. A study was initiated in this area and it was found that, when the reduced solution lies on a state-variable inequality constraint boundary, the boundary layer trajectories are of finite time in the stretched time scale. The possibility of costate discontinuites at the juncture between constrained and unconstrained arcs makes direct application of existing theory difficult at best. A transformation technique was identified that eliminates some of these difficulties, but at the cost of possibly increased system order and the introduction of singular arcs. Much work remains to be done in this area.

Work on development of simple, efficient algorithms for prediction of vehicle aerodynamic and propulsive performance have continued during the present phase of the program. Improvements in modeling of the hypersonic lifting body module have eliminated previous discrepancies between measured and predicted aerodynamic behavior. Several modes of data entry are now implemented making assessment of a given vehicle configuration very simple. An interactive program mode has been devised that makes possible direct and immediate assessment of configuration changes on selected vehicle performance paramaters. The algorithms developed in this program are of potential use in applications beyond those originally envisioned.

Four conference papers have now been published which discuss most of the results of this research effort. A Ph.D. Dissertation that details the entire effort to date was published in Decemeber of 1989. A full-length paper entitled "Rapid Near-Optimal Trajectory Generation for Single-Stage-to-Orbit Airbreathing Vehicles" has been submitted for publication in the AIAA Journal of Guidance, Control and Dynamics and a new paper is now being prepared for the 1990 AIAA GN&C Conference on the issue of state contraints in singularly perturbed systems.

Table of Contents

List of Figures

List of Symbols

c_j = thrust specific fuel consumption for engine type j
C_1 = inequality constraint, dynamic pressure
C_2 = inequality constraint, aerodynamic heating
C_3 = inequality constraint, tangential acceleration
C_4 = inequality constraint, normal acceleration
C_{D_o} = zero-lift drag coefficient
$C_{L\alpha}$ = lift curve slope
D = aerodynamic drag
E = mass specific energy
F_C = thrust component aligned with the velocity vector
F_S = thrust component normal to the velocity vector
f = total fuel flow rate
f_{max_i} = combined fuel flow rate for any number of independent engines of type i when operating at a stoichiometric fuel-to-air ratio
g = acceleration due to gravity at mean sea level
h = altitude, given by $r - r_E$
H = Hamiltonian function
J = performance index
K = coefficient of the lift induced drag component
L = aerodynamic lift
m = vehicle mass
M = Mach number
n = total number of different engine cycles employed
n-p = number of engine types employed for which fuel flow rate varies in direct proportion to φ but thrust varies in a nonlinear fashion with φ
n_1 = component of acceleration aligned with the velocity vector
n_2 = component of acceleration normal to the velocity vector
p = number of engine types employed that exhibit linear dependence of both fuel flow rate and thrust on η
q = dynamic pressure
Q = aerodynamic heating rate per unit area
r = radial distance from the center of the Earth
r_E = mean sea level
s = aerodynamic reference area
S_j = switching function for bang-bang control of η_j
t = time
t_f = final time
T = net thrust
T_k = combined thrust of any number of independent engines of type k, k=1 to p
U = pseudo control variable
V = velocity
W = Vehicle weight, taken at mean sea level (W = mg)
α = angle of attack
α_{ZL} = angle of attack for zero lift
γ = flight path angle
δ_e = elevon deflection

ε = perturbation parameter, 0 or 1

ε_{T_k} = angle between T_k and the body longitudinal axis

η_j = throttle control, engine type j

λ_x = costate, subscript denotes related state

μ = gravitational constant for the Earth

ρ = atmospheric density

σ = bank angle

τ = transformed time variable, $\tau = t/\varepsilon$

φ_i = fuel equivalence ratio, engine type i

π = vector containing control for each engine type

SECTION 1
Introduction

Emerging technology in many engineering fields, including hypersonic air-breathing propulsion, computational fluid dynamics, and high temperature materials, may soon make possible a vehicle configuration that has been the subject of study for over four decades[1]. This vehicle concept is commonly referred to as an aerospace plane. Its development, in one version or another, is being pursued by a number of industrialized nations. The current U.S. concept consists of a single-stage vehicle propelled, for the most part, by airbreathing engines. Most notable among the airbreathing cycles to be employed is that of the supersonic combustion ramjet or "scramjet." This aircraft is to be fueled by liquid hydrogen and will take-off and land horizontally on conventional runways. Operational objectives include hypersonic cruise in the upper atmosphere for long durations and the ability to accelerate to orbital velocity. Potential missions for such a vehicle include transportation to low-Earth-orbit, intercontinental passenger transportation, and a wide range of defense missions. This research effort is focused upon the particular mission of single-stage-to-orbit which promises, by the use of air-breathing hypersonic propulsion and greatly reduced launch operations, an order of magnitude reduction in the cost of placing payloads in low Earth orbit [2,3].

Even with the greatly improved fuel efficiency of airbreathing propulsion over current rocket engine technology, the ability to attain orbit in a single-stage vehicle will be marginal at best[4]. Trajectory optimization will play an important role in mission success for this reason. In fact, because the airbreathing propulsion system characteristics are sensitive to vehicle attitude and atmospheric conditions, precise trajectory control will be required. State-of-the-art launch vehicle guidance technology is heavily reliant on pre-mission, ground-based trajectory generation/optimization. In order to be cost effective, aerospace plane operations will have to approach those of modern commercial airlines. Technology dependent upon pre-mission, ground-based trajectory optimization is inadequate for this task; real-time, on-board trajectory optimization will be required[5].

The state of the art in trajectory optimization for complex nonlinear systems consists of a number of well developed numerical methods of solution. Unfortunately, these algorithms are poorly suited for on-board, real-time implementation. They are, in general, computationally intense, require an initial guess of the solution, and are lacking in global convergence characteristics. While some success in designing a reliable algorithm to numerically solve a two

point boundary value problem in an on-board computer has been achieved for orbit transfer[6], the diverse mission requirements and complex control structure of a general purpose aerospace plane will likely require that structured methods for order reduction be employed.

Energy state approximations and singular perturbation methods have been successfully employed to derive near-analytic trajectory optimization algorithms in the past. Near-optimal feedback guidance laws have also been obtained. These methods also contribute considerable insight into the nature of the optimal profiles and their relation to vehicle aerodynamic and propulsion characteristics. Early studies were devoted to fighter aircraft performance optimization[7-9]. However, many of the modeling approximations employed for analysis of subsonic and supersonic aircraft optimal trajectories are not valid for a vehicle with hypersonic cruise and orbital capabilities.

This research report presents an analysis of the problem of fuel-optimal ascent to low-Earth-orbit of an airbreathing, single-stage-to-orbit vehicle. Section II presents the problem formulation. A generic multi-mode propulsion system is defined which incorporates turbojet, ramjet, scramjet, and rocket engines. Inequality constraints on dynamic pressure, aerodynamic heating rate, and vehicle acceleration are also introduced. In Section III an algorithm for generating fuel-optimal climb profiles is derived employing an energy state approximation. This algorithm results from application of the minimum principle to a low order dynamic model that includes general functional dependence on angle of attack and a normal component of thrust. Switching conditions are derived which, under appropriate assumptions, govern optimal transition from one propulsion mode to another. The use of bank angle to modulate the magnitude of the vertical component of lift is also investigated. A nonlinear transformation technique is employed to derive a feedback controller for tracking the computed trajectory. Section IV provides an overview of the vehicles models employed in this work. Section V provides a presentation and discussion of representative numerical results, and Section VI states conclusions drawn from this work. The main body of the report is followed by two appendices. Appendix A details an initial investigation into the characteristics of boundary layer systems when the reduced solution lies on a state-variable inequality constraint boundary. Appendix B details work performed in analytical vehicle model development.

SECTION 2

General Problem Formulation

Consider atmospheric flight of a point mass over a spherical non-rotating Earth. The equations governing such flight can be reduced to a four state model as follows,

$$\dot{E} = \frac{V(F_C - D)}{m} \tag{1}$$

$$\dot{m} = -f(r,E,\pi,\alpha) \tag{2}$$

$$\dot{\varepsilon\gamma} = \frac{(F_S + L)\cos\sigma}{mV} - \frac{\mu\cos\gamma}{Vr^2} + \frac{V\cos\gamma}{r} \tag{3}$$

$$\dot{\varepsilon r} = V\sin\gamma \tag{4}$$

The perturbation parameter, ε, which has been artificially inserted, is nominally one. It is assumed that the atmosphere is stationary and that the thrust vector lies in the vehicle's plane of symmetry. In (1), mass specific energy, E, is employed as a state variable in place of velocity, V, where

$$E = V^2/2 - \mu/r \tag{5}$$

The reference point for zero gravitational potential is taken at a radial distance approaching infinity. The symbol V is to be taken as

$$V = [2(E + \mu/r)]^{1/2} \tag{6}$$

everywhere it appears in this analysis. Position and heading dynamics are decoupled from (1–4) by the assumption of a non-rotating Earth and are not of interest at present.

Drag is assumed to have a conventional parabolic form

$$D = qsC_{D_o} + KL^2/qs \qquad \text{where} \qquad q = \rho V^2/2 \tag{7}$$

The assumed functional dependence for C_{D_o} , the zero lift drag coefficient, and K, the coefficient of the induced drag component, are:

$$C_{D_o} = C_{D_o}(M) \qquad K = K(M,\alpha) \tag{8}$$

Lift is given by

$$L = qsC_L(r,E,\alpha,\delta_e) = qsC_{L\alpha}(\alpha - \alpha_{ZL}) \tag{9}$$

The lift curve slope, $C_{L\alpha}$, and the angle of attack for zero lift, α_{ZL} , are assumed to be Mach number dependent.

A multi-mode propulsion system composed of n different engine types (i.e. cycles) is assumed. Net thrust is given by

$$T = [\, F_C^{\,2} + F_S^{\,2} \,]^{1/2} \tag{10}$$

where F_C represents the component of net thrust along the velocity vector and F_S represents the component of net thrust normal to the velocity vector, i.e. in the lift direction. These components are depicted in Figure 1 and given by:

$$F_C = \sum_{j=1}^{p} \eta_j T_j \cos(\alpha + \varepsilon_{T_j}) + \sum_{i=p+1}^{n} T_i \cos(\alpha + \varepsilon_{T_i}) \tag{11}$$

$$F_S = \sum_{j=1}^{p} \eta_j T_j \sin(\alpha + \varepsilon_{T_j}) + \sum_{i=p+1}^{n} T_i \sin(\alpha + \varepsilon_{T_i}) \tag{12}$$

Each of the n engine cycles (i.e. turbojet, ramjet, scramjet, rocket, etc.) is controlled by variation of the fuel flow rate in direct proportion to command. Of the total number of engine types to be considered, p are assumed to exhibit a linear relation between fuel flow rate and thrust generation. Each engine of this type shall be controlled by varying its throttle setting, η_j. This assumption is typically employed for rocket engines. For the remaining n–p engine cycles, the relation between fuel flow rate and thrust generation is assumed nonlinear. Control of each engine of this type shall be effected by variation in its fuel equivalence ratio, φ_i. This behavior is typical of air-breathing cycles. The subscripted symbol T_k (k = 1 to n) in (11) and (12) represents the net thrust generated

by any number of independent engines employing a particular cycle k. The symbol ε_{T_k} denotes the angle between T_k and the body longitudinal axis (see Figure 1). Note that in general,

$$T_j = T_j(r,E,\alpha) \qquad \eta_j \in [0,1] \qquad j = 1 \text{ to } p \tag{13}$$

$$T_i = T_i\,(r,E,\varphi_i,\alpha) \qquad \varphi_i \in [0,1] \qquad i = p+1 \text{ to } n \tag{14}$$

$$\varepsilon_{T_k} = \varepsilon_{T_k}(r,E,\alpha) \qquad k = 1 \text{ to } n \tag{15}$$

The total fuel flow rate, f, is given by

$$f = \sum_{j=1}^{p} \eta_j\, c_j(r,E,\alpha)\, T_j(r,E,\alpha) + \sum_{i=p+1}^{n} \varphi_i\, f_{max_i}(r,E,\alpha) \tag{16}$$

where c_j represents the thrust specific fuel consumption for engine type j and f_{max_i} represents the product of thrust specific fuel consumption and thrust at a stoichiometric fuel-to-air ratio for engine type i. For convenience all of the engine throttle controls are collected into a single vector as follows,

$$\pi^T = [\eta_1, \eta_2, \ldots, \eta_p, \varphi_{p+1}, \ldots, \varphi_n] \tag{17}$$

The control variables are angle of attack, α, bank angle, σ, the fuel equivalence ratios, φ_i, for engine types 1 through n, and engine throttle settings, η_j, for engine types n+1 through p. The objective is to minimize the fuel consumed in gaining energy, with the performance index given by,

$$J = -\,m(t_f) \tag{18}$$

The final time, t_f, is free. Minimization of (18) is to be carried out subject to maximum dynamic pressure and maximum aerodynamic heating rate inequality constraints and acceleration limits defined by

$$C_1\,(r, E) = q - q_{max} \leq 0 \tag{19}$$

$$C_2 (r, E, \alpha) = Q - Q_{max} \leq 0 \tag{20}$$

$$C_3 (r, E, m, \alpha, \pi) = n_1 - n_{1max} \leq 0 \tag{21}$$

$$C_4 (r, E, m, \alpha, \pi) = n_2 - n_{2max} \leq 0 \tag{22}$$

The symbols n_1 and n_2 represent the accelerations in g's along and normal to the velocity vector (i.e. in the lift direction), respectively.

SECTION 3

Singular Perturbation Analysis

3.1 Reduced Solution.

Lift as a Control. We first consider a simplified problem in which flight is constrained to a vertical plane, the thrust vector is aligned with the velocity vector, and thrust production is assumed independent of vehicle angle of attack:

$$\sigma = 0, \qquad F_S = 0, \qquad F_C = T \tag{23}$$

Furthermore, we consider only that portion of the trajectory in the hypersonic regime. In this regime we need only consider a dual-mode propulsion system (i.e. n = 2). The system consists of a bank of scramjet engine modules assumed to operate continuously and a rocket engine that can be throttled as desired. The constraint (21), which can lead to the requirement for intermediate values of throttle setting, will be ignored. In this simplified setting the total fuel flow rate and net thrust can be represented as

$$T = T_s(r,E) + \eta\, T_r(r) \quad ; \quad \eta \in [0,1] \tag{24}$$

$$f = c_s(r,E)\, T_s + \eta\, c_r(r)\, T_r \tag{25}$$

where thrust specific fuel consumption is represented by c_s for the scramjet and c_r for the rocket. Under these assumptions the governing equations of motion can be written as,

$$\dot{E} = \frac{V(T-D)}{m} \tag{26}$$

$$\dot{m} = -f\,(r,E,\eta) \tag{27}$$

$$\varepsilon\dot{\gamma} = \frac{L}{mV} - \frac{\mu \cos\gamma}{Vr^2} + \frac{V\cos\gamma}{r} \tag{28}$$

$$\varepsilon\dot{r} = V\sin\gamma \tag{29}$$

The control variables are now rocket engine throttle, η, and vehicle lift, L. The objective remains to minimize the fuel consumed in gaining energy.

Setting $\varepsilon = 0$ in (26-29) reduces the order of the dynamic system to two and results in what is conventionally referred to as the energy state approximation. That is, altitude and flight path angle dynamics are assumed fast in comparison to energy and mass dynamics, and altitude now takes on the role of a control variable[9]. The differential equations (28) and (29) are reduced to algebraic equations which yield the following relations:

$$\gamma_o = 0 \tag{30}$$

$$L_o = m[(\mu/r^2) - (V^2/r)] \tag{31}$$

The subscript zero denotes reduced solution values and is omitted below where not deemed necessary for clarity. The reduced solution Hamiltonian is given by

$$H_o = \lambda_E \dot{E} + \lambda_m \dot{m} + \text{constraints} = 0 \tag{32}$$

where

$$\lambda_m (t_f) = -1.0 \tag{33}$$

Satisfaction of the minimum principle with respect to altitude, h, is equivalent to the following operation (see Appendix B of reference 10),

$$h_o^* = \arg\max_h [V(T-D)/f] \Big|_{\substack{E = \text{constant} \\ T > D \quad q \le q\max \\ \eta = \eta^* \quad Q \le Q\max}} \tag{34}$$

Consideration of the constraints (19, 20) simply limits the search space over which the maximization of (34) takes place. The superscript asterisk denotes an optimal value of control. This operation yields an optimal altitude program as a function of vehicle energy and mass. Note that η appears linearly in the Hamiltonian resulting in a bang-bang control solution for rocket throttle setting. A switching condition, S, results from the evaluation of $\partial H_o/\partial \eta$ and is given by,

$$S = \lambda_E(V/m) - \lambda_m c_r \tag{35}$$

Using (32) to eliminate λ_E in (35) and taking into account the sign of λ_m† yields the following analytic switching condition:

$$\eta = 0 \quad \text{if} \quad [(c_r - c_s)/c_r]T_s > D$$
$$\eta = 1 \quad \text{if} \quad [(c_r - c_s)/c_r]T_s < D \tag{36}$$

Intermediate values of rocket throttle setting are not optimal. This fact is revealed by examination of the matrix H_{uu}, which is required to be at least positive semidefinite along an optimizing singular arc. For convenience, V, rather than h is taken as the control-like variable so that $u^T = [\, V, \eta \,]$. The determinant of H_{uu}, which is symmetric, must be greater than or equal to zero for positive semidefiniteness. However, it can be shown that

$$\det H_{uu} = -\left\{H_{V\eta}\right\}^2 \tag{37}$$

which is negative for $H_{V\eta} \neq 0$, which is generally the case.

It can happen that the velocity set is not convex in a region of interest, and, in the absence of convexity, one can not guarantee that an optimal control exists. Thus the possibility of a chattering control solution should be examined. Conclusions regarding this matter are model dependent and are discussed in reference 16. It is sufficient to say here that no chattering solutions for rocket throttle setting were found for the vehicle models examined.

The reduced solution costates are determined as[12]:

$$\lambda_{r_o} = 0 \qquad \lambda_{m_o} \equiv -\, m(t_f)/m \tag{38}$$

$$\lambda_{\gamma_o} = \lambda_{E_o}\,[2KV^2L_o/(qs)] \qquad \lambda_{E_o} = \lambda_{m_o}\,\{fm/[V(T-D)]\} \tag{39}$$

---

† The "influence function", λ_m, represents the variation in the performance index, J, with respect to mass[11]. Since $J = -\, m(t_f)$, λ_m cannot change sign (i.e. it is not possible for a reduction in vehicle mass as fuel is expended along the climb path to increase the final mass of the vehicle).

Angle of Attack as a Control. Consider now the full model complexity formulated in Section II with the exception that flight remains constrained to a vertical plane. That is, consider flight over the entire Mach range, including the subsonic and supersonic regimes. Assume a multi-mode propulsion system consisting of turbojet, ramjet, scramjet, and rocket cycles (i.e. n = 4). Allow for a component of net thrust normal to the velocity vector and consider the possibility that the performance of one or more of the air-breathing engine cycles is dependent on vehicle angle of attack. Consider also the constraint on axial acceleration given by (21). The method of solution proceeds as before.

Setting $\varepsilon = 0$ in (1-4) reduces the differential equations (3) and (4) to algebraic relations:

$$\gamma_o = 0 \tag{40}$$

$$L_o = m(\mu/r^2 - V^2/r) - F_S \tag{41}$$

The control α_o is eliminated via (41). That is, given values of r and E, α_o is iteratively determined using (41) while enforcing trim through elevon deflection, δ_e. More concisely,

$$\alpha_o(r,E) = \{\alpha_o: L(r,E,\alpha,\delta_e) - L_o(r,E,\pi,\alpha) = 0\} \tag{42}$$

The reduced solution Hamiltonian is again given by (32). But since drag, given by (7), is dependent on L_o^2, which in turn depends on engine controls through F_S, as given in (12), the φ_i and the η_j both enter nonlinearly in the Hamiltonian. Satisfaction of the minimum principle with respect to h and π is equivalent to the following operation,

$$h_o^*, \pi^* = \arg\max_{h,\pi} [V(F_C - D)/f] \Big|_{\substack{E = \text{constant} \quad Fc > D \\ q \le q\max \quad Q \le Q\max \\ n_1 \le n_{1\max} \quad n_2 \le n_{2\max}}} \tag{43}$$

This operation yields both an optimal altitude program as a function of vehicle energy and mass and the corresponding optimal engine controls.

If we neglect the dependence of reduced solution drag on the sine component of net thrust, F_S, then the η_j enter linearly in H_o. In such case we have bang-bang solutions for the η_j with possible

singular arcs along which intermediate throttle settings may be optimal. The switching functions are determined as before from $\partial H_o/\partial \eta_j$,

$$S_j = [f(\pi)\cos(\alpha + \varepsilon_{T_j})/(F_C(\pi) - D)] - c_j \qquad j = 1+n \text{ to } p \tag{44}$$

Throttle settings are then governed by the following relations:

$$\begin{array}{lll} \eta_j = \eta_{min} & \text{if} & S_j < 0 \\ \eta_j \text{ singular} & \text{if} & S_j = 0 \text{ for finite time} \\ \eta_j = \eta_{max} & \text{if} & S_j > 0 \end{array} \tag{45}$$

The S_j are dependent on the η_k, $k \neq j$. Thus an iterative scheme is required to arrive at the optimal combination of throttle settings if $j > 1$.

Thus far in the analysis it has been assumed that each engine cycle can be independently controlled. Since much of the captured mass flow and some or all of the engine hardware will be shared by the various engine cycles employed, it is perhaps more useful to consider operation of the various air-breathing cycles as mutually exclusive. In reality, dual combustion over a finite range of Mach number will be required to smoothly transition from subsonic to supersonic combustion[13]. One can view the case of mutually exclusive engine cycles as a problem in which the system equations are discontinuous at cycle transition points along the trajectory. Following the terminology of reference 11, suppose that one set of system equations,

$$\dot{x} = f^{(1)}(x,u,t) \tag{46}$$

applies for $t < t_1$, where t_1 is free, and another set of system equations applies for $t > t_1$, namely,

$$\dot{x} = f^{(2)}(x,u,t) \tag{47}$$

Here x and u denote general state and control vectors, respectively. It is necessary for optimality that

$$H^{(1)}(t_1-) = H^{(2)}(t_1+) \tag{48}$$

The condition (48) can be used to determine the optimal point of transition from one set of system equations to another. In this case $f^{(1)}$ and $f^{(2)}$ differ only by the thrust produced by the particular engine cycle being employed and by the associated difference in fuel consumption. Satisfaction of

(48) can be reduced to the following equality where the condition $H_o = 0$ has been employed to eliminate costate dependence

$$(T_i \cos(\alpha + \varepsilon_{T_i}) - D)/c_i T_i = (T_j \cos(\alpha + \varepsilon_{T_j}) - D)/c_j T_j \qquad (49)$$

This result is, in fact, obvious from examination of (43). That is to say, points at which a change in engine cycle can occur require that the function to be maximized be equal for either choice of the propulsion cycle. When the functional evaluations are not equivalent, one or the other is greater and dictates the optimal choice of cycle.

Bank Angle as a Control. It is reasonable to assume that the performance of the proposed scramjet engines will be sensitive to vehicle angle of attack. Furthermore, it is quite likely that thrust production will depend on angle of attack in a nonlinear way. Given that this is true, any particular engine installation will exhibit an angle of attack for which engine performance is best. This angle of attack for best engine performance, call it the design angle of attack, may in turn vary with Mach number[14]. If such nonlinear behavior is assumed and the optimal flight path is constructed using (43), one finds that, since fuel optimization is very sensitive to engine performance, the optimal trajectory tends to remain on a contour along which the design angle of attack is maintained. It can happen, however, that overall performance is improved if the design angle of attack is maintained while flying at lower altitudes, and hence at higher values of dynamic pressure. Of course, maintaining the design angle of attack at a higher dynamic pressure generates additional lift which causes the vehicle to immediately climb above the desired flight path. Thus, in order to fly along the optimal path, the extra lift associated with maintaining the design angle of attack must be "dumped." One procedure for accomplishing this task is to roll back and forth in such a way that, on average, the component of lift in the vertical direction is reduced to that required to maintain the optimal climb rate. It may in fact be more practical to appropriately offset the initial vehicle heading and to then execute a single coordinated turn that accomplishes the same objective. With bank angle thus introduced as an additional control, satisfaction of the minimum principle with respect to h, π, and α is equivalent to the following operation,

$$h_o^*, \pi^*, \alpha_o^* = \arg\max_{h,\pi,\alpha} [V(F_C - D)/f] \Big|_{\substack{E = \text{constant} \quad Fc > D \\ q \le q_{max} \quad Q \le Q_{max} \\ n_1 \le n_{1max} \quad n_2 \le n_{2max}}} \qquad (50)$$

where bank angle, σ, is determined so that

$$L \cos \sigma = L_o \tag{51}$$

3.2 Boundary Layer Analysis.

The unconstrained boundary layer solution associated with (1–4) is obtained by introducing the time transformation $\tau = t/\varepsilon$ and again setting $\varepsilon = 0$. That is, energy and mass are held constant while altitude and flight path angle dynamics are examined on a stretched time scale. The resulting necessary conditions for optimality yield an optimal feedback guidance law for lift control which depends on the unknown costate λ_γ (see Section 5.2.2 of reference 10). In the absence of a state inequality constraint such as (19), a suitable approximation to λ_γ can be obtained by linearizing the boundary layer necessary conditions about the reduced solution[10,15]. However, this procedure is not applicable when the reduced solution lies on a state constraint boundary. This problem is discussed in detail in Appendix A. The boundary layer control solutions for engine throttle settings are similar to those of the reduced solution. The η_j enter the Hamiltonian linearly, but the switching conditions that govern their behavior are also dependent on the unknown costate λ_γ. This dependence drops out of the switching conditions if the sine component of thrust, F_S, is neglected.

Feedback Linearization - Lift as a Control. As an alternative approach to handling the control of altitude and flight path dynamics, a nonlinear transformation technique is employed as follows[10]. Consider the boundary layer altitude and flight path angle dynamics given in (32) and (33) on a transformed time scale $\tau = t/\varepsilon$. Note that we have system equations in block triangular form. To proceed we take successive total time derivatives of r until explicit dependence on the control appears. The prime notation denotes differentiation with respect to τ.

$$r'' = (L\cos\gamma)/m + (V^2 \cos^2\gamma)/r - (\mu/r^2) \tag{46}$$

The control, L, appears in the second time derivative and we define U, the pseudo control, as

$$U = r'' \tag{47}$$

It is desired that U be determined as follows

$$U = K_p\left(r_o - r\right) + K_d\left(\dot{r}_o - r'\right) \tag{48}$$

where r_o denotes the reduced solution radius at the current energy level and the time derivative of r_o denotes the climb rate required to stay on the reduced solution as energy is gained. This climb rate can be estimated by defining an appropriate increment in energy, evaluating the reduced solution at this higher energy level, and then estimating the required climb rate using a forwards difference.

The inverse transformation is defined by solving for L in (47) using (46) and (48),

$$L = \{U + (\mu/r^2) - [(V^2/r)\cos^2\gamma]\}(m/\cos\gamma) \tag{49}$$

This lift control solution is constrained directly by (21). Note that as r and γ approach their reduced solution values, (49) approaches the reduced solution value of lift given by (35). A block diagram depicting the conceptual implementation of the nonlinear transformation technique to yield the controller defined by (49) is presented in references 10, 15 and 16. The corresponding closed loop transfer function is

$$G(s) = (K_d s + K_p)/(s^2 + K_d s + K_p) \tag{50}$$

where the gains K_p and K_d for the second order system can be written in terms of the damping ratio, ζ, and natural frequency, ω_n, as

$$K_p = \omega_n^2 \qquad K_d = 2\zeta\omega_n \tag{51}$$

The performance of this controller can be dictated by selecting the values of K_p and K_d to yield the desired dynamic response. This lift control solution applies equally well to the unconstrained or the inequality constrained case.

Feedback Linearization - Angle of Attack as a Control. Direct extension of the lift control solution presented above to include the angle of attack effects included in (1-4) results in the following feedback control law,

$$\alpha^* = \left\{ \alpha : \left[U + \frac{\mu}{r^2} - \frac{V^2 \cos^2 \gamma}{r} \right] \frac{m}{\cos \gamma} - (F_S + L) = 0 \right\} \tag{63}$$

The pseudo-control, U, is defined as before where again K_p, proportional gain, and K_d, rate gain, are selected to yield the desired controller performance. Optimal lift, which is directly constrained by (21), is then determined by,

$$L^* = qsC_{l_\alpha} (\alpha^* - \alpha_{ZL}) \tag{64}$$

SECTION 4
Vehicle Models

Four different vehicle models were employed to generate the numerical results presented in the next section. The first, referred to as Model 1, is based on a hypersonic research vehicle concept studied by NASA in the 1970's and is powered by a combination of scramjet and rocket propulsion[10]. This model is useful only in the hypersonic regime. Models 2 and 3 are based on a "Generic Hypersonic Aerodynamic Model Example," or GHAME, developed more recently by NASA[17]. A nominal configuration of 233.4 feet total length and 300,000 pounds gross take-off weight was assumed. The trimmed aerodynamic characteristics were taken directly from the GHAME documentation. For Model 2 the largely empirical GHAME I aerodynamic data set was employed. For Model 3 the numerically generated GHAME II aerodynamic data set was employed. Both sets extend from take-off to orbital velocities. Thrust for both Models 2 and 3 is provided by a multi-mode propulsion system composed of turbojet, ramjet, scramjet, and rocket engines. The airbreathing propulsive characteristics for this model were adopted from reference 18. A rocket, sized for orbital insertion (roughly 15,000 lbs. of thrust in vacuum), is assumed available over the entire Mach range[10]. This system corresponds to the case p = n = 4 in (11), (12), and (16). As a result, the switching conditions given by (45) can be used to determine all of the cycle transition points. Figure 2 presents the adopted variation in fuel specific impulse with Mach number for the various engine cycles. The various engines where sized by trial and error and do not represent an optimal configuration. The generation of scramjet thrust due to mass ejection when operating above a stoichiometric fuel-to-air ratio is not modeled. Thrust induced pitching moments, which can be significant[16], were not considered when trimming the aircraft. A fourth model was constructed by combining an aerodynamic data set provided by the NASA Langley Research Center (referred to as the "Langley Accelerator") with the propulsive data described above. Additional details regarding these models are available in references 10 and 19.

A simple model for convective heating rate per unit area, Q, was adopted from reference 20,

$$Q = (4.919\ \text{E-}08)\ \rho^{0.5}\ V^{3.0} \qquad (52)$$

Equation (52) gives Q in Watts/cm^2 given density in kg/m^3 and velocity in m/sec and corresponds to equilibrium conditions on the surface of a sphere or wing leading edge 10 cm in radius and cooled by reradiation alone. For reference, a contour of Q = 800 in the altitude-velocity plane corresponds roughly to a contour along which skin temperature remains at approximately 2000° F three feet aft of the leading edge assuming laminar flow[21].

SECTION 5
Numerical Results

Reduced solution trajectories were generated by carrying out the maximization process indicated in (34), (43), and (50) over the energy range from take-off to orbit. Numerous results are available in reference 19. Only a few representative plots are presented here. Figure 3 depicts reduced solution trajectories for Model 1 in the altitude/velocity plane. Dynamic pressure is limited to 2000 psf while maximum allowable heating rate is varied. The trajectories follow the dynamic pressure constraint boundary until the specified contour of maximum heating rate is encountered. The path then follows the constant heating rate contour until reaching the trajectory for which no heating rate constraint was enforced. At this point the heating constraint becomes inactive and the trajectory rejoins the unconstrained climb path. The mechanism causing the altitude discontinuity at a velocity of 22,000 ft./sec. is similar to that which has been noted in the transonic region for supersonic fighter aircraft[15]. Included in Figure 3 is the rocket switching surface, i.e. the contour along which the switching function (39) remains zero. At altitudes below this contour the optimal rocket throttle setting is zero whereas above the contour the optimal throttle setting is one. The performance penalty paid in enforcing the heating constraint is presented in Figure 3 as time required and percent gross weight consumed to achieve an orbital energy level. This performance penalty must be weighed against the complications of using active cooling, the weight of heat shielding, and various other factors in the vehicle design process.

Figure 4 presents the reduced solution climb path in the altitude-velocity plane for Vehicle Model 4. The dynamic pressure constraint is again enforced, an aerodynamic heating constraint is not, and a limit on axial acceleration is introduced. The trajectories vary predictably as the magnitude of the acceleration constraint is changed. Some throttling of the engines is employed but in general the vehicle prefers instead to climb to reduce the excess thrust available. Note that the altitude discontinuity present in Figure 3 does not occur for this vehicle, but is in fact implicit in matching a terminal altitude condition at orbital velocity. The horizontal bars at the top of the figure indicate the velocity range over which the operation of each engine cycle was deemed optimal, including regions of cycle overlap. The rocket operation was not optimal during atmospheric flight for this case.

Computational investigations of the sensitivity of scramjet performance to changes in angle of attack predict highly nonlinear behavior[14]. Figure 5 presents a scramjet thrust scaling factor employed to model this effect. This figure is based on a liberal interpretation of the computational

results presented in reference 14. This curve is shifted with respect to the horizontal axis in order to represent inlet designs which favor maximum engine performance at an angle of attack other than zero.

Figure 6 presents variations in the dynamic pressure constrained reduced solution trajectories for Model 3 when thrust variation with angle of attack for both the ramjets and scramjets, as depicted in Figure 5, is included. The angle of attack for best engine performance is varied over the range from 0.5 to 3.0 degrees. When only scramjets are operating, the vehicle tends to prefer a path along which the "design" angle of attack is strictly maintained. The performance penalty paid for a change in the design angle of attack is modest however, since in this Mach region, the acceleration capability of the vehicle is high. When the thrust scaling factor of Figure 5 is assumed Mach dependent in accordance with the results of reference 14, a much greater variation in the trajectory is experienced[19].

The peak in the trajectories at approximately 3000 ft./sec. in Figure 6 is due to turbojet shut down. This peak is significantly reduced when the turbojet inlet area is increased, indicating that the climb away from the dynamic pressure constraint boundary is due to the decreasing level of thrust available from the turbojet as the Mach number increases. With an increase in altitude comes a reduction in vehicle drag, but the turbojet switching surface is encountered at an altitude of approximately 75,000 ft. and the turbojet shut down. The SCRAMJET almost immediately switches on, and with a much greater magnitude of thrust, can sufficiently overcome vehicle drag, even at a higher dynamic pressure. Thus the trajectory returns to the dynamic pressure constraint boundary. Note that the ramjet is turned on at a very low Mach number (i.e. M = 0.81) even though it is extremely inefficient in this speed range (see Figure 2). This behavior has been noted by past researchers and is due to the presence of a "pinch point" (i.e. a point of minimum thrust minus drag) in the transonic region. The size of the ramjet was selected without regard to its weight. However, optimization of the vehicle configuration must take into account the mass of each engine and the mass of the required engine cowling. Results obtained indicate that the optimal trajectory for such an optimized configuration may prefer the use of rocket (rather than ramjet) thrust to augment turbojet thrust at the transonic pinch point.

As stated above, cycle operations are represented in Figure 6 by horizontal bars. The transition points were very nearly the same for thrust independent of or dependent on angle of attack. The overlap in air-breathing cycles is desirable to provide smooth cycle transitions. For Model 3, turbojet sizing requires about 25 sq. ft. of inlet area, whereas the total number of ramjet modules selected require 200 sq. ft. of inlet area. Thus it should be possible to start the majority of the

ramjet engines in a sequence that avoids excessive accelerations while maintaining turbojet thrust. Once the velocity for turbojet shut-down is reached, turbojet airflow can be diverted to the remaining ramjet modules. The number of required scramjet modules is likewise larger than the number of required ramjet modules, and a similar argument for cycle overlap can be made. Of course, the actual system will no doubt share much of the engine hardware amongst the various cycles employed in addition to sharing the captured mass flow. Thus the actual optimization of engine transitions will be more complex.

Modulation of the vertical component of lift via bank angle variation was also evaluated for Model 3. Carrying out the maximization process indicated in (50) alters the trajectories presented in Figure 6 only slightly. The changes correspond to those portions of the trajectory where $\alpha_o < \alpha_{design}$. As such, only a very modest gain in performance was achieved. However, if design constraints force the scramjet design angle of attack to differ significantly from the angle of attack for zero lift, much greater savings can be obtained.

Figure 7 depicts the reduced solution trajectory for Vehicle Model 2 in the altitude-velocity plane. A maximum allowable dynamic pressure of 2000 psf is the only constraint enforced. The dashed line labeled 1 represents the fuel-optimal climb path when scramjet performance is assumed independent of vehicle angle of attack. The percent of take-off gross weight consumed in attaining orbital energy is 61. The solid line label 2 represents the fuel-optimal climb path when scramjet performance is assumed to vary with angle of attack according to Figure 5, with optimum engine performance assumed to occur at an angle of attack of 3 degrees across the Mach range. In this case the trajectory tends to remain on the dynamic pressure constraint boundary for the majority of the flight. The percent of take-off gross weight consumed in attaining orbital energy in this case is 68.2. The weight penalty of 7.2 percent of the take-off gross weight most likely exceeds the payload capability of the vehicle. This comparison indicates the critical need to accurately model the many interactions present among disciplines.

Figure 8 depicts the altitude time history for simulated flight of Model 3 using the lift control law derived via feedback linearization to track the corresponding reduced solution. The ramjet cycle was eliminated and the trajectory is subjected to the following constraints: dynamic pressure $\leq$ 2000 psf, reference heating rate $\leq$ 400 Watts/cm^2, and axial acceleration $\leq$ 3.0 g's. In general this vehicle preferred to climb in order to satisfy an axial acceleration limit rather than to throttle back the engines. The rapid climb at roughly 400 seconds is due to scramjet turn-on and this preferred behavior. The large overshoot just before 500 seconds is due to the inability of the vehicle to pull down as the altitude for which $n_1 \leq 3$ at full throttle is approached. This overshoot

can be reduced somewhat by careful gain scheduling and having the controller look ahead in energy. However, the requirement to fine tune the controller for each trajectory generated is *not* desirable for the intended applications of this algorithm. The problem has less to do with the controller than with the generation of the trajectory itself.

Over the vast majority of the trajectory the flight path angle is small and the flight path angle rate very modest so that (41) provides a good approximation to the actual lift required to follow the flight trajectory. However, when the scramjet is initially turned on at a relatively high value of dynamic pressure, the energy rate of the vehicle is greatly increased. The necessity of simultaneously climbing to avoid violating the dynamic pressure constraint boundary results in a large flight path angle rate. The time scale separation assumed in (1-4) is simply not appropriate over this small portion of the trajectory. A simple way to overcome this difficulty consists of estimating the flight path angle and time interval between energy levels, combining them to form an estimate of the flight path angle rate, and then inverting relation (3) to obtain the required lift. By restricting the accelerations normal to the flight path when constructing the reduced solution in this region, a feasible trajectory can always be obtained.

Figure 9 depicts the reduced solution climb path for Model 3 again with a maximum dynamic pressure of 2000 psf, a maximum aerodynamic heating rate of 400 Watts/cm^2, but with a maximum axial acceleration of 1g to amplify the problem ($\gamma = 0$ in the lift calculations). Also depicted is the modified trajectory when the method described above is implemented (γ and $d\gamma/dt \neq 0$). The results in the altitude/velocity plane are quite dramatic over the speed range from 3,000 to 12,000 ft./sec. The near vertical altitude transition at a velocity of approximately 3,000 ft./sec. is eliminated, as is the dive that followed. The arc which follows in the velocity range from 5,000 to 13,000 ft./sec. corresponds to the region over which the axial acceleration limit is active. Less altitude change is commanded in this region; more throttle is used to reduce the axial acceleration instead. The remainder of the trajectory, the same for either case, constitutes flight along the heating constraint boundary. Despite the significant change in trajectory, only 200 additional pounds of fuel are consumed and the difference in time of flight is only about 60 seconds. These small differences are due to the fact that the velocity interval from 3,000 to 12,000 ft./sec. is traversed very rapidly in time, corresponding to only a small fraction of the total time of flight.

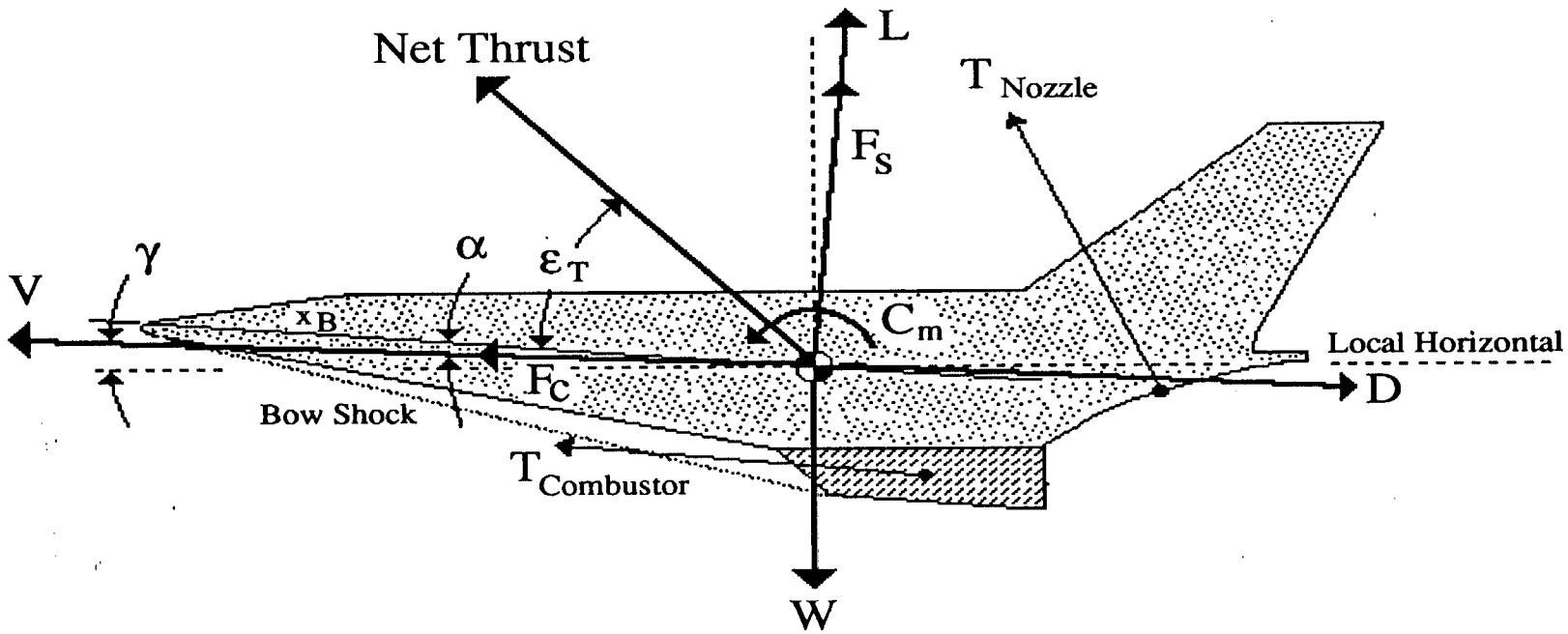

Figure 1 Partial Force and Moment Diagram

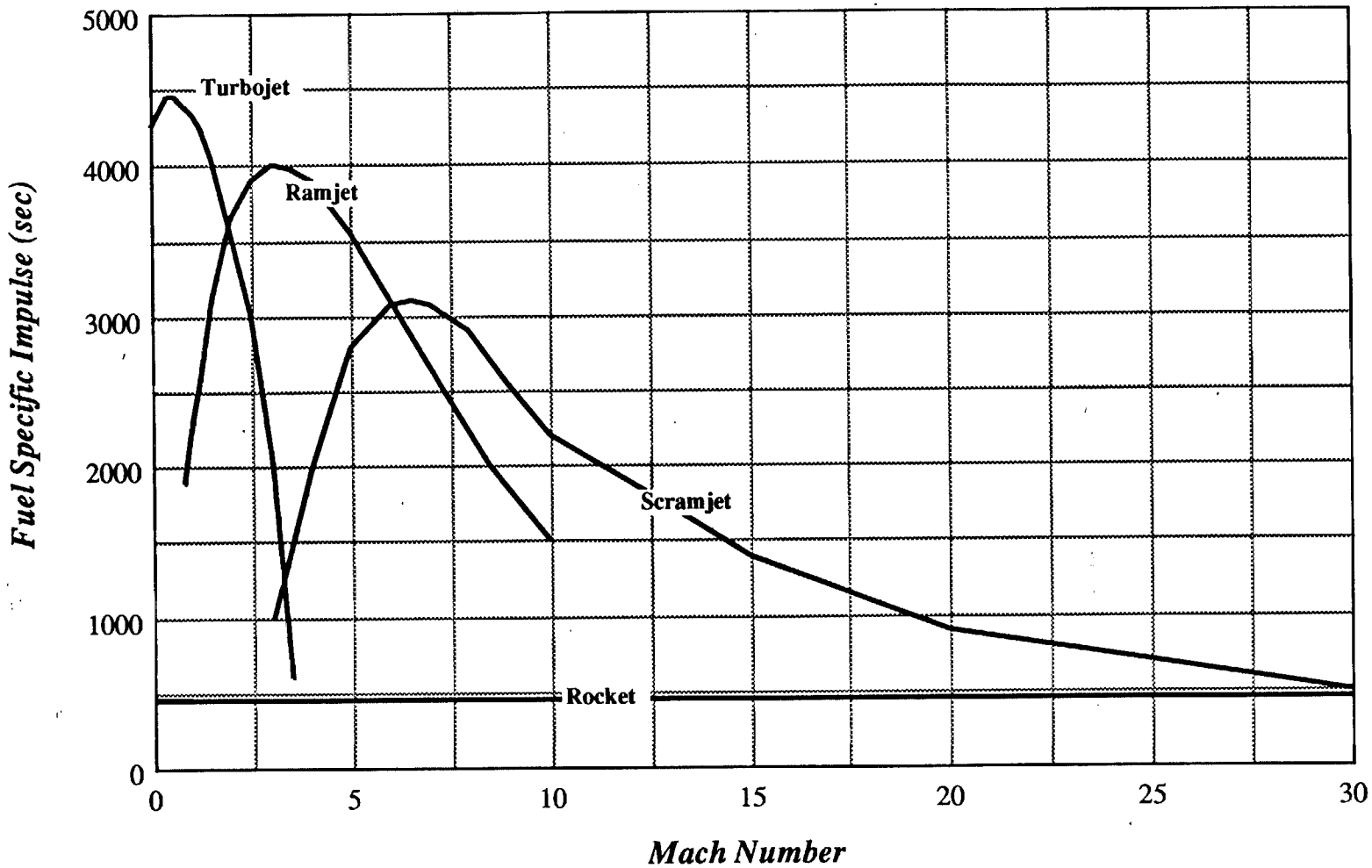

Figure 2 Fuel specific impulse versus Mach number for the various propulsion cycles available to Vehicle Models 2 through 4.

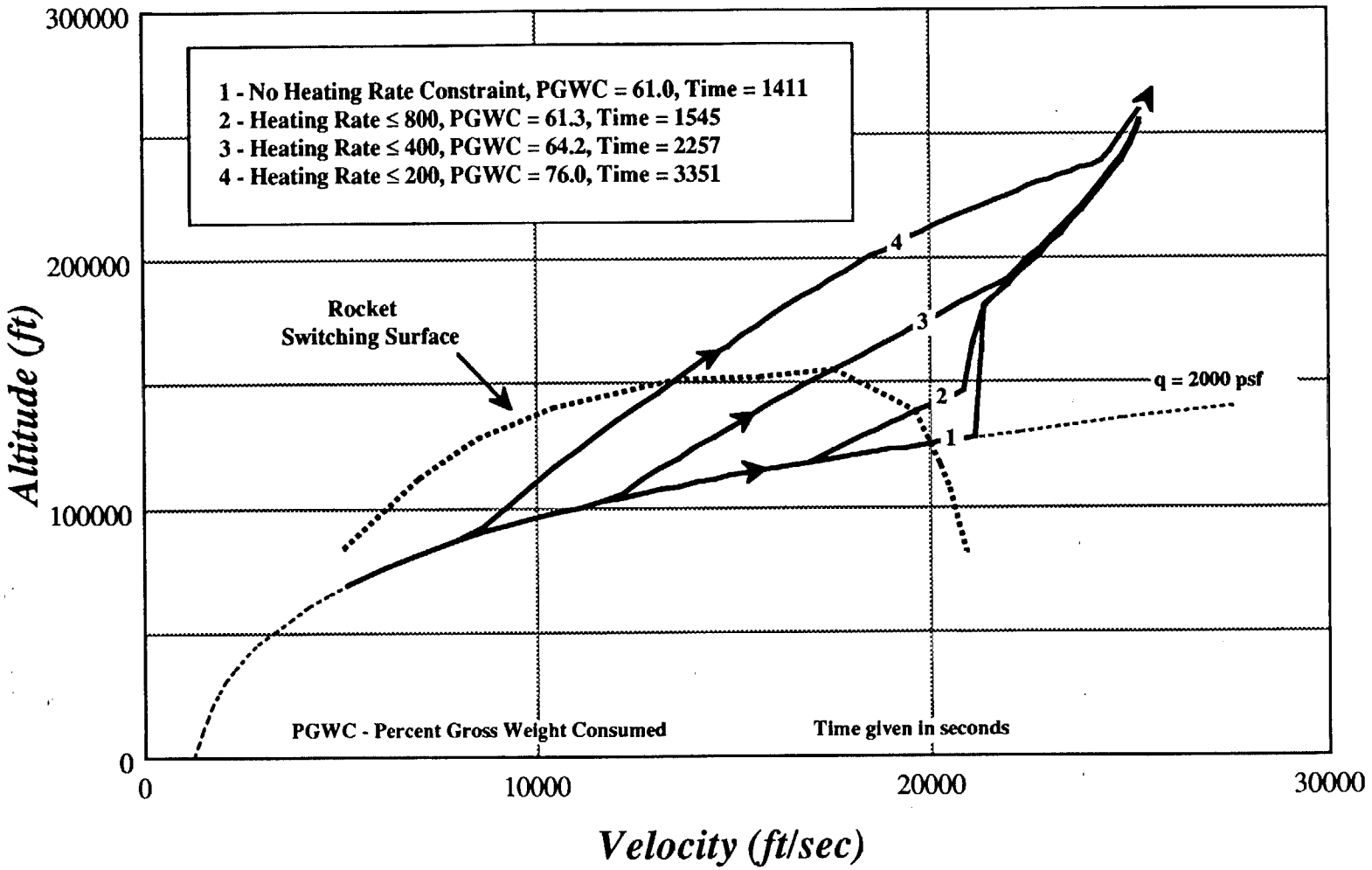

Figure 3 Reduced Solution for Vehicle Model Number 1 as the maximum aerodynamic heating rate constraint (shown in Watts/cm²) is varied.

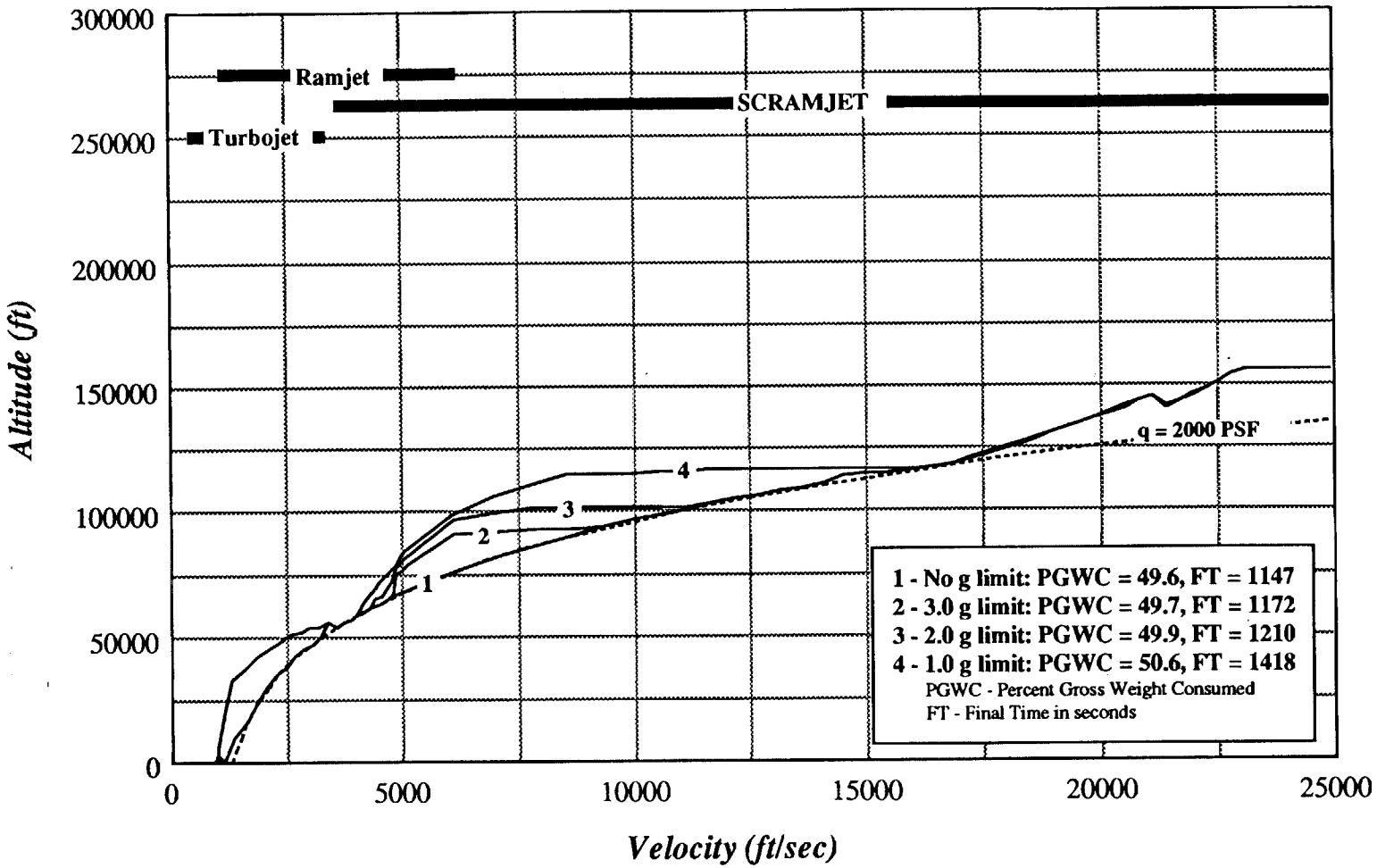

Figure 4 Reduced Solution for Vehicle Model Number 4; variation in the magnitude of the axial acceleration constraint is shown.

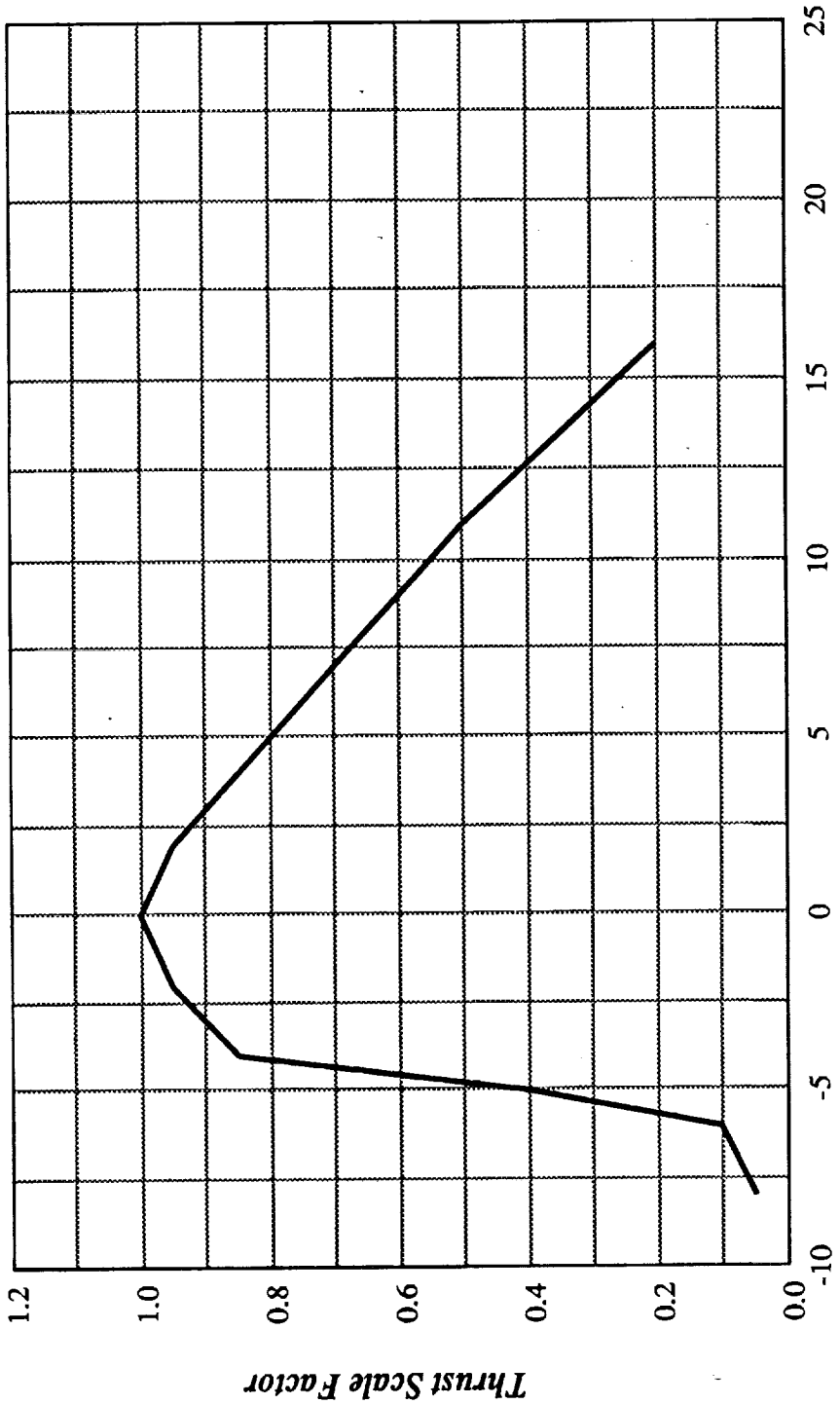

Figure 5 Assumed variation in scramjet thrust with angle of attack.

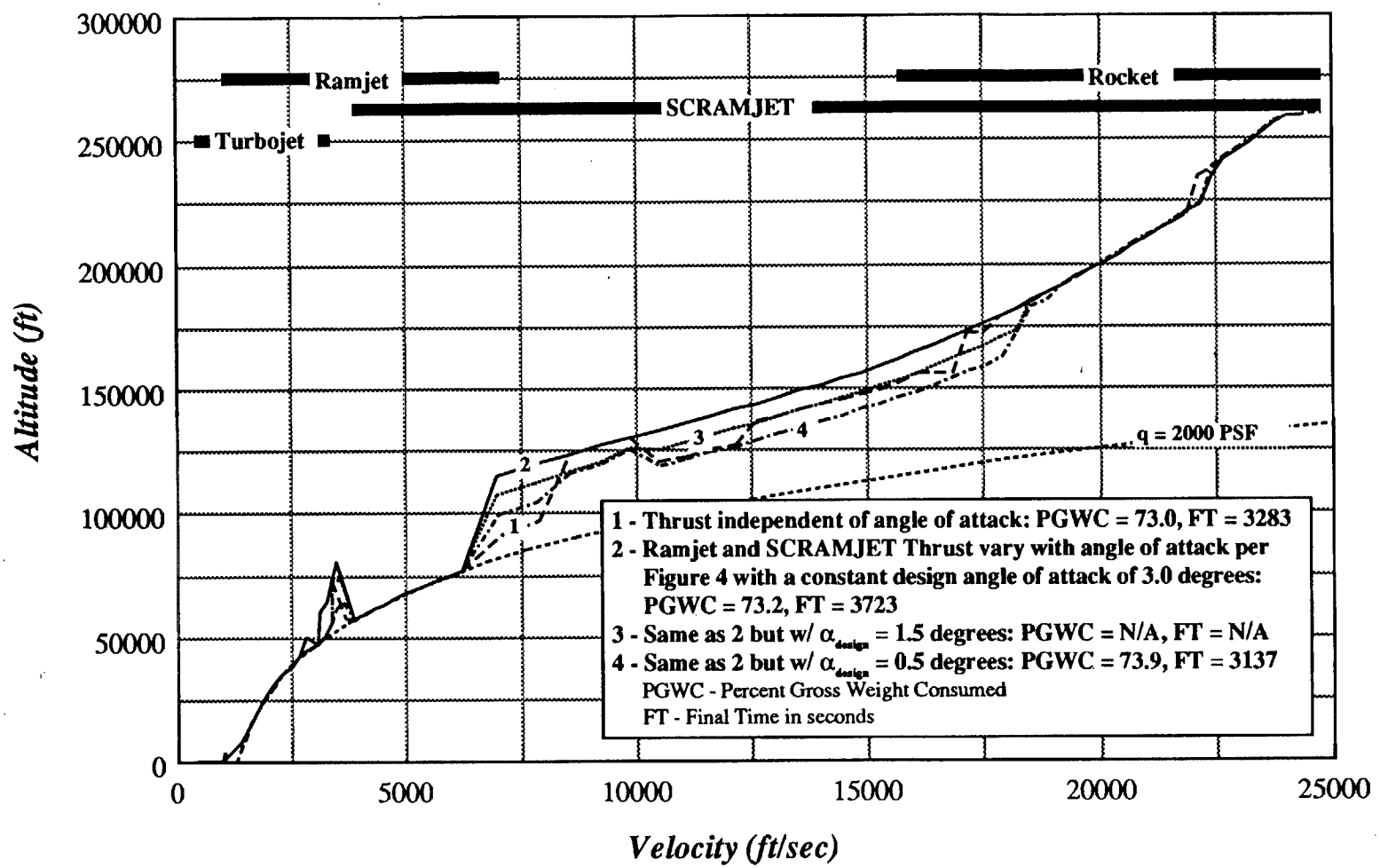

Figure 6 Reduced Solution for Vehicle Model Number 3; the effect of thrust variation with angle of attack is shown as the design angle of attack is varied.

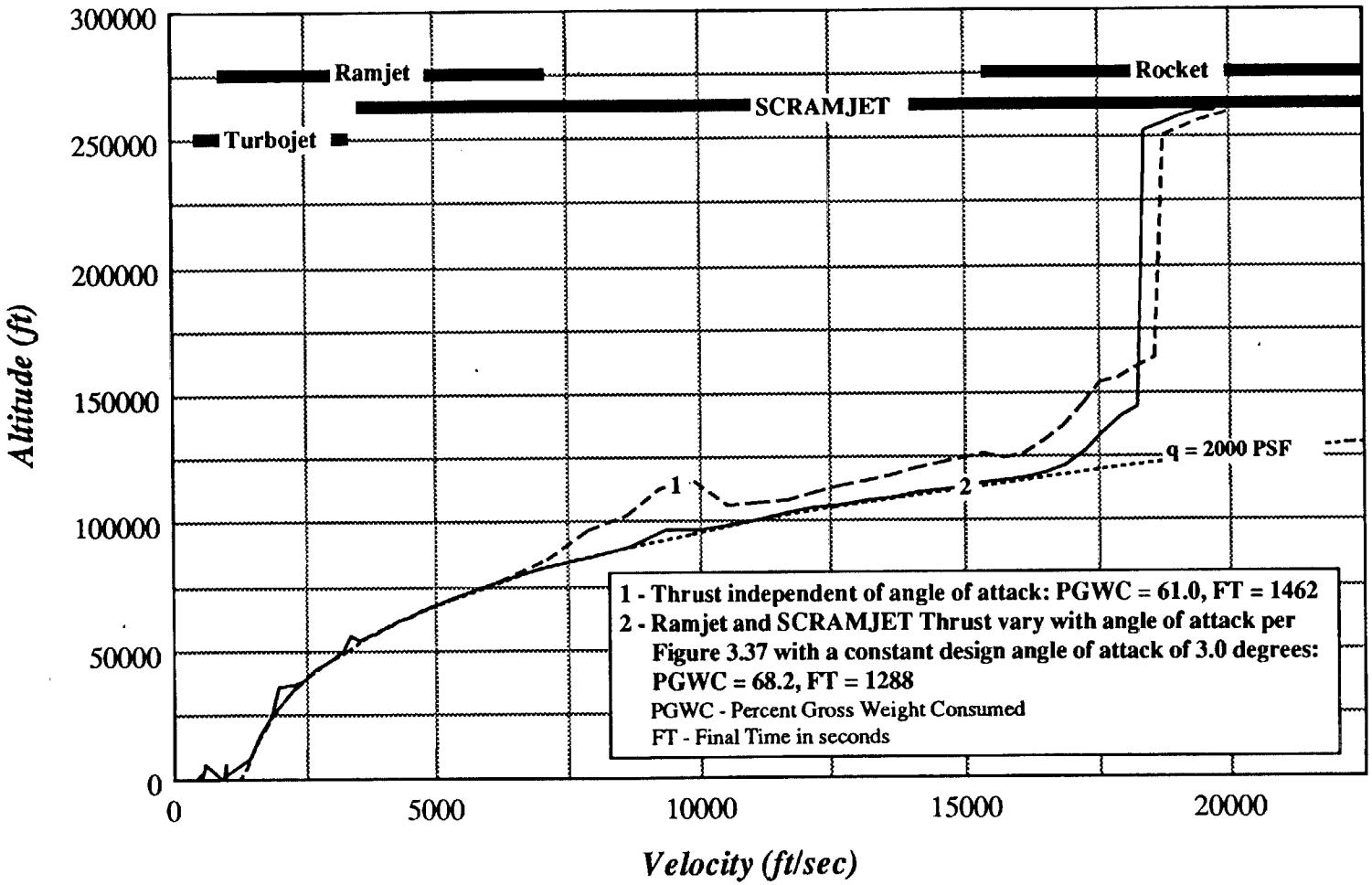

Figure 7 Reduced Solution for Vehicle Model Number 2; the effect of thrust variation with angle of attack is shown.

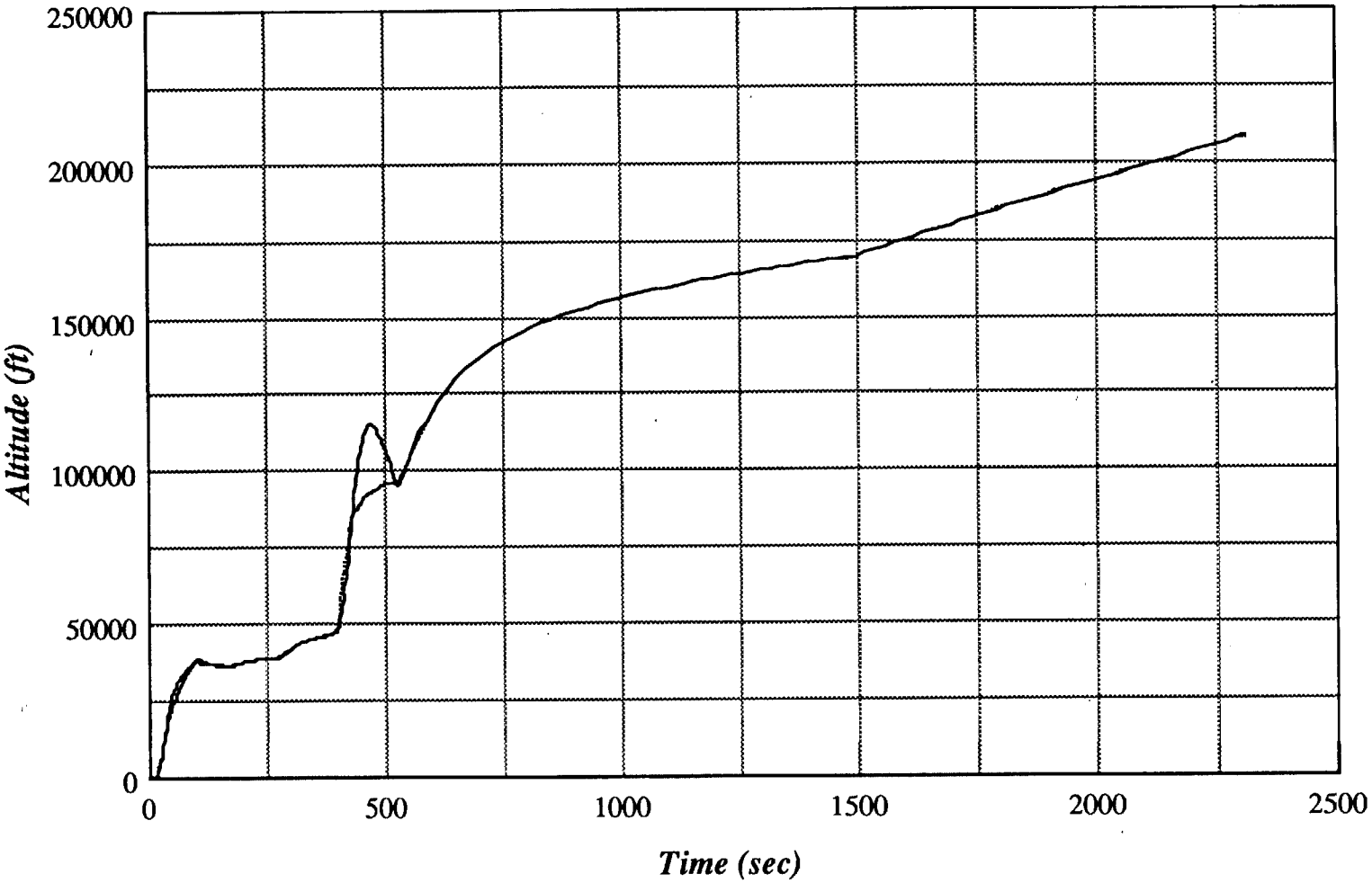

Figure 8 Guided solution for Model 4; altitude time history.

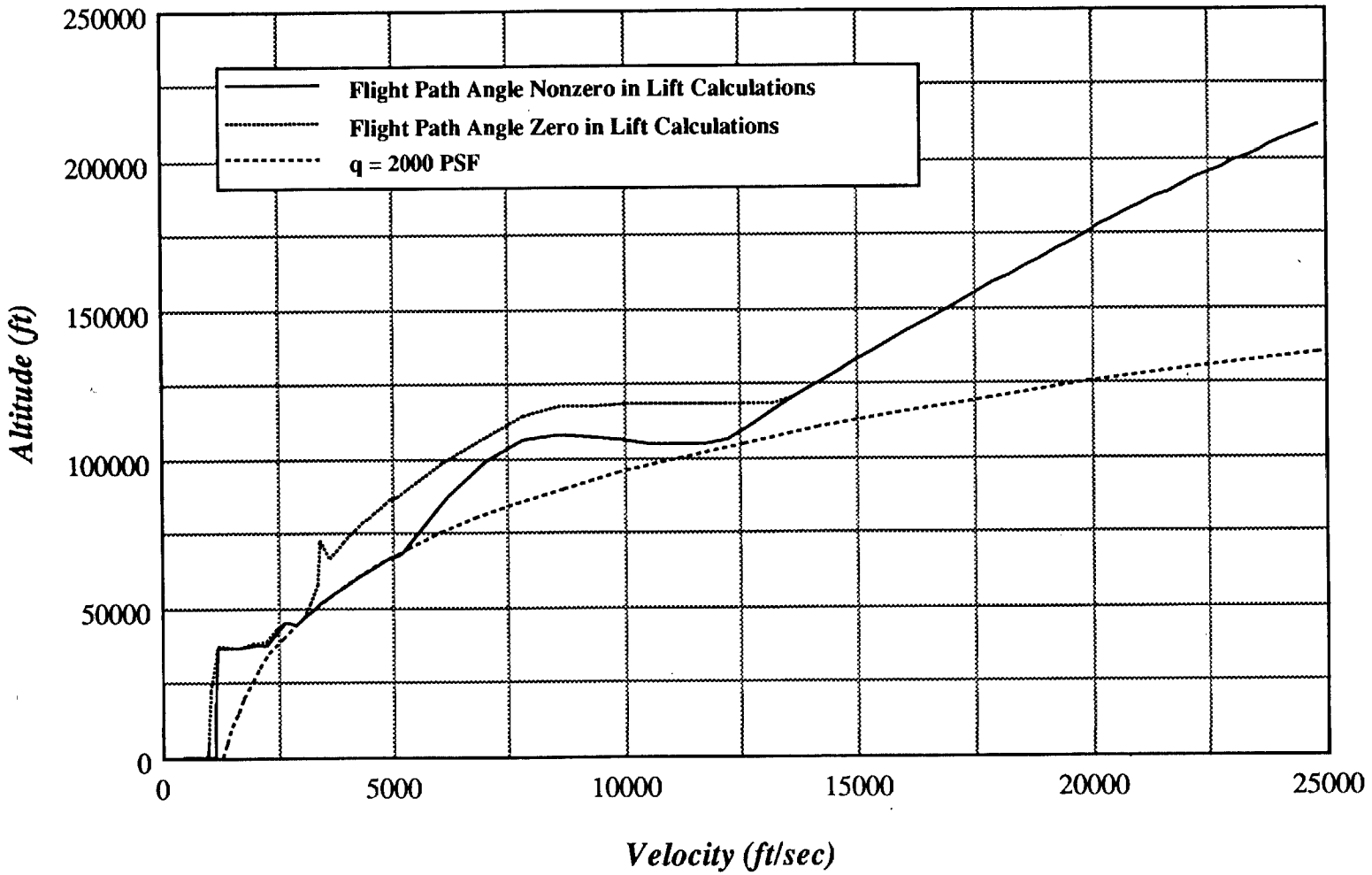

Figure 9 Reduced Solution for Model 4; comparison of the trajectory when flight path angle and flight path angle rate are included in the calculation of lift with the trajectory when they are not included.

SECTION 6
Conclusions and Recommendations

6.1 Conclusions

This research effort has demonstrated the utility of singular perturbation methods in the study of single-stage-to-orbit airbreathing vehicles and, in particular, in the derivation of efficient algorithms for ascent trajectory optimization and optimization of engine cycle transitions. The analysis extends over the entire Mach range from take-off to orbit and accomodates a realistic nonlinear vehicle model and all pertinent trajectory constraints. A number of important modeling and analysis issues not treated in the early stages of this effort were identified and addressed during this reporting period. Reasonable assumptions regarding propulsion system characteristics were introduced that allow the optimal engine cycle transition points to be determined as a function of state using a simple iterative test. These switching conditions lead to significant computational savings during the optimization process. Functional dependence of scramjet thrust on vehicle angle of attack was shown to have a major impact on the nature of fuel-optimal ascent trajectories. Also, depending on the actual vehicle configuration and the characteristics of the engine inlets, roll maneuvers used to modulate the vertical component of lift were shown to sometimes improve the index of performance during ascent. Over those limited regions of flight where the energy state approximation was found to be poor, simple lift corrections that account for non zero flight path angle and flight path angle rate were introduced that significantly improve the trajectory generation methodology.

6.2 Recommendations

Future efforts should be directed towards enhancing the performance and applicability of the derived algorithm. Such efforts should include the development of detailed multi-disciplinary vehicle models, the incorporation of additional controls such as thrust vectoring, reaction jets, and variable geometry, optimal control of the total heat load on the vehicle, the study of three-dimensional maneuvers, including abort, an examination of robustness issues, and improvements in speed of operation.

The demonstrated capability for rapid near-optimal trajectory generation has yet to be exploited in the development of efficient tools for fully integrated hypersonic vehicle design. Efforts to move in this direction should include tieing a parameter optimization algorithm around the trajectory optimization code that has been developed and the incorporation of this algorithm into a fully integrated control system design methodology.

Work of more general theoretical interest was also initiated during this reporting period. It was found that state-variable inequality constrained boundary layer systems are not well understood. Many of the characteristic features of such systems were identified. For instance, it was found that, when the reduced solution lies on a state-variable inequality constraint boundary, the boundary layer trajectories are of finite time in the stretched time scale. The possibility of costate discontinuites at the juncture between constrained and unconstrained arcs makes direct application of existing theory difficult. A transformation technique was identified that eliminates some of these difficulties, but at the cost of possibly increased system order and the introduction of singular arcs. Further research in this area is recommended.

Continued work with the integrated aerodynamic/propulsion performance prediction program has resulted in a highly accurate and useful means both for providing the needed vehicle parameters in the present program and for more general transatmospheric flight performance calculations. The program is evolving into a completely interactive performance estimation package, which will make it possible to view effects of small configuration changes on any performance parameters. The user can view in animated graphical form the effect of desired vehicle configuration changes. These modifications can be entered graphically by moving defining points on the vehicle outlines or by means of shifting simulated "levers" built in to the computer program. For example wing incidence angle, twist, wing area, fin cant angle, etc. can be changed continuously with simultaneous graphical output showing the effect on selected performance parameters. We anticipate many applications for this analytical capability and will continue to improve upon it.

6.3 Publications

Four conference papers have now been published which discuss most of the results of this research effort[12,15,16,49]. A Ph.D. Dissertation that details the entire effort to date was published in Decemeber of 1989[19]. A full-length paper entitled "Rapid Near-Optimal Trajectory Generation for Single-Stage-to-Orbit Airbreathing Vehicles" has been submitted for publication in the AIAA Journal of Guidance, Control and Dynamics and a new paper is now being prepared for the 1990 AIAA GN&C Conference on the issue of state contraints in singularly perturbed systems.

References

[1]Heppenhiemer, T. A., "Keepers of the Flame," *AIR & SPACE/Smithsonian*, Vol.4, No. 5, Dec. 89/Jan. 90, pp. 88-95.

[2]*National Aero-Space Plane, A Technology Development and Demonstration Program to Build the X-30*, United States General Accounting Office Report to Congressional Committees, GAO/NSIAD-88-122, April 1988.

[3]Williams, R. M., "National Aero-space Plane: Technology for America's Future," *Aerospace America*, Vol. 24, No. 11, Nov. 1986, pp. 18-22.

[4]Gregory, T. J., "Credibility of NASP," *Aerospace America*, Vol. 27, No. 9, Sept. 1989, pp. 42-46.

[5]Hardtla, J. W., Piehler, M. J., and Bradt, J. E., "Guidance Requirements for Future Launch Vehicles," AIAA Paper 87-2462, Aug. 1985.

[6]Bradt, J. E., Hardtla, J. W., and Cramer, E. J., "An Adaptive Guidance Algorithm for Aerospace Vehicles, AIAA Paper 85-1917, Aug. 1985.

[7]Bryson, A. E., Jr., "Energy-State Approximation in Performance Optimization of Supersonic Aircraft," *Journal of Aircraft*, Vol. 6, Nov.-Dec. 1969, pp. 481-488.

[8]Kelley, H. J., "Flight Path Optimization with Multiple Time Scales," *Journal of Aircraft*, Vol. 8, April 1971, pp. 238-240.

[9]Calise, A. J., "Extended Energy Management Methods for Flight Performance Optimization," *AIAA Journal*, Vol. 15, March 1977, pp. 314-321.

[10]Calise, A. J., Corban, J. E., and Flandro, G. A., "Trajectory Optimization and Guidance Law Development for National Aerospace Plane Applications," Final Report for Period July 1, 1987 to November 30, 1988, NASA Contract Number NAG-1-784, December 1988.

[11]Bryson, A. E., Jr., and Ho, Yu-Chi, *Applied Optimal Control*, Hemisphere Publishing Corp., New York, 1975.

[12]Calise, A. J., Corban, J. E., and Flandro, G. A., "Trajectory Optimization and Guidance Law Development for National Aerospace Plane Applications," Proceedings of the 1988 ACC, Vol. 2, June 15-17, Atlanta, GA, pp. 1406-1411.

[13]Kandebo, S. W., "Pratt Demonstrates Low-Speed Propulsion Concept for National Aero-Space Plane," *Aviation Week & Space Technology*, p. 79, June 26, 1989.

[14]Walton, J., "Performance Sensitivity of Hypersonic Vehicles to Changes in Angle of Attack and Dynamic Pressure," AIAA Paper No. 89-2463.

[15]Corban, J. E., Calise, A. J., and Flandro, G. A., "Trajectory Optimization and Guidance Law Development for Transatmospheric Vehicles," Proceeding of the 1989 IEEE International Conference on Control and Applications (ICCON), April 3-6, Jerusalem, Israel.

[16]Corban, J. E., A. J. Calise, and G. A. Flandro, "Optimal Guidance and Propulsion Control for Transatmospheric Vehicles," AIAA Paper 89-3617, Aug. 1989.

[17]Bowers, A. H. and Iliff, K. W., "A Generic Hypersonic Aerodynamic Model Example (GHAME) for Computer Simulation," A proposed NASA Technical Note, Ames Research Center, June, 1988.

[18]Waltrup, P. J., Anderson, G. Y., and Stull, F. D., "Supersonic Combustion Ramjet (SCRAMJET) Engine Development in the United States," Preprint 76-042, The 3rd International Symposium on Air Breathing Engines, The Johns Hopkins University Applied Physics Laboratory, March, 1976.

[19]Corban, J. E., "Real-Time Guidance and Propulsion Control for Single-Stage-to-Orbit Airbreathing Vehicles," Ph.D. Dissertation, The Georgia Institute of Technology, December 1989.

[20]Tauber, M. E., G. P. Menees, and H. G Adelman, "Aerothermodynamics of Transatmospheric Vehicles," AIAA-86-1257, AIAA/ASME 4th Joint Thermophysics and Heat Transfer Conference, Boston, Mass., June 2-4, 1986.

[21]Johnston, P. J., A. H. Whitehead, Jr., and G. T. Chapman, "Fitting Aerodynamics and Propulsion into the Puzzle," *Aerospace America*, September 1987, pp 32-37 and 42.

[22]Jacobson, D. H., M. M. Lele, and J. L. Speyer, "New Necessary Conditions of Optimality for Control Problems with State-Variable Inequality Constraints," Journal of Mathematical Analysis and Applications, 35, pp. 255-284, 1971.

[23]Kreindler, E., "Additional Necessary Conditions for Optimal Control with State-Variable Inequality Constraints," Journal of Optimization Theory and Applications," Vol. 30, No. 2, Oct. 1982, pp. 241-251.

[24]Boykin, W. H., Jr., and T. E. Bullock, "State Constraints and Singular Solutions to Penalty Function Optimization Problems," AIAA Journal, Vol. 10, No. 2, Feb. 1972, pp. 137-141.

[25]Calise, A. J., "On the Use of Singular Perturbation Methods in the Solution of Variational Problems," Proceedings of the Joint Automatic Controls Conference, Columbus, Ohio, 1973, pp. 184-192.

[26]Calise, A.J., Moerder, D.D., "Singular Perturbation Techniques for Real Time Aircraft Trajectory Optimization and Control," NASA Contractor Report 3597, August, 1982.

[27]Falco, M. and H. J. Kelly, "Aircraft Symmetric Flight Optimization," Control and Dynamic Systems, Advances in Theory and Applications, Vol. 10, Academic Press, New York, NY, 1973. (see Figure 14 on page 114)

[28]McHenry, R. L., T. J. Brand, A. D. Long, B. F. Cockrell, and J. R. Thibodeau III, "Space Shuttle Ascent Guidance, Navigation, and Control," *The Journal of the Astronautical Sciences*, Vol. XXVII, No. 1, pp. 1-38, January-March, 1979.

[29]Hargraves, C. R., and S. W. Paris, "Direct Trajectory Optimization Using Nonlinear Programming and Collocation," *Journal of Guidance*, Vol. 10, No. 4, July-August 1987, pp. 338-342.

[30]Jacobson, D. H. and M. M. Lele, "A Transformation Technique for Optimal Control Problems with a State Variable Inequality Constraint," *IEEE Transactions on Automatic Control*, Vol. AC-14, No. 5, Oct. 1969, pp. 457-464.

[31]Calise, A. J. and J. E. Corban, "Optimal Control of Singularly Perturbed Nonlinear Systems with State Variable Inequalty Constraints," presented at the IFAC Workshop on Singular Perturbations and Asymptotic Methods in Systems and Control, Boston, MA, August 17-18, 1989.

[32]McIntyre, J. and B. Paiewonsky, "On Optimal Control with Bounded State Variables," Advances in Control Systems, Theory and Applications, Vol. 5, Academic Press, New York, NY, 1967.

[33]Bryson, A. E., Jr., W. F. Denham, and S. E. Dreyfus, "Optimal Programming Problems Problems with Inequality Constraints I: Necessary Conditions for Extremal Solutions," *AIAA Journal*, Vol. 1, No. 11, Nov. 1963, pp. 2544-5550.

[34]Denham, W. F. and A. E. Bryson, Jr., "Optimal Programming Problems Problems with Inequality Constraints II: Solution by Steepest Ascent," *AIAA Journal*, Vol. 2, No. 1, Jan. 1964, pp. 25-34.

[35]Speyer, J. L., "Nonlinear Feedback Solution to a Bounded Brachistchrone Problem in a Reduced State Space," IEEE Transactions on Automatic Control, Feb. 1967, pp. 90-94.

[36]Speyer, J. L. and A. E. Bryson, Jr., "Optimal Programming Problems with a Bounded State Space, " AIAA Journal, Vol. 6, No. 8, pp. 1488-1491, Aug. 1968.

[37]Taylor, J. G., "Comments on a Multiplier Condition for Problems with State Variable Inequality Constraints," IEEE Transactions on Automatic Control, Oct. 1972, pp. 743-744.

[38]Hamilton, W. E., Jr., "On Nonexistence of Boundary Arcs in Control Problems with Bounded State Variables," IEEE Transactions on Automatic Control, Vol. AC-17, No. 3, June 1972, pp. 338-343.

[39]Russak, I. B., "Second Order Necessary Conditions for Problems with State Inequality Constraints," SIAM Journal of Control, Vol. 13, No. 2, Feb. 1975, pp. 372-388.

[40]Maurer, H., "On Optimal Control Problems with Bounded State Variables and Control Appearing Linearly," SIAM Journal of Control and Optimization, Vol. 15, No. 3, May 1977, pp. 345-362.

[41]Lowen, P. D., "State Constraints in Optimal Control"

[42]Ardema, M. D., "Singular Perturbations in Flight Mechanics," NASA TM X-62, 380, Aug. 1974; Revised July 1977.

[43]Ardema, M. D., "Linearization of the Boundary Layer Equations of the Minimum Time to Climb Problem," Journal Guidance and Control, Vol. 2, No. 5, pp. 434-436.

[44]Shankar, U. J., E. M. Cliff, and H. J. Kelly, "Singular Perturbation Analysis of Optimal Climb-Cruise-Dash," AIAA Guidance and Control Conference, Monterey, CA, August 17-19, 1987.

[45]Weston, A. R., Cliff, E. M., and H. J. Kelly, "Altitude Transitions in Energy Climbs," *Automatica*, Vol. 19, No. 2, pp. 199-202, 1983.

[46]Ardema, M. D., "Nonlinearly Singularly Perturbed Optimal Control Problems with Singular Arcs."

[47]Heck, B. S., and A. H. Haddad, "Singular Perturbation Analysis for Linear Systems with Vector Quantized Control," Proceedings of the 1989 American Control Conference, Pittsburgh, PA, June 21-23, pp. 2178-2183.

[48]Conversation with A. J. Calise and Eyad H. Abed of the University of Maryland at the 1989 AIAA GN&C Conference, Boston, MA, Aug. 14-16, 1989.

[49]Corban, J. E., Calise, A. J., and Flandro, G. A., "A Real-Time Guidance Algorithm for Aerospace Plane Optimal Ascent to Low Earth Orbit," Proceeding of the 1989 American Control Conference (ACC), June 21-23, Pittsburgh, Pa.

Appendix A

State Inequality Constrained Boundary Layers

Abstract

The established necessary conditions for optimality in nonlinear control problems that involve state-variable inequality constraints are applied to a class of singularly perturbed systems. The distinguishing feature of this class of systems is a transformation of the state-variable inequality constraint, present in the full order problem, to a constraint involving states and controls in the reduced problem. It is of particular interest to construct the zeroth order boundary layer solution when the reduced solution lies on the constraint boundary. It is shown that, in general, the boundary layer problem is of finite time in the stretched time variable. A special case is identified in which the boundary layer time scale transformation results in an increase in state inequality constraint order. In this case, required smoothness properties possessed by the full order system may be lost, and the application of existing necessary conditions for singularly perturbed systems then becomes invalid. A Valentine transformation can be used to regain required smoothness, but at the price of introducing singular arcs and an increase in system order. Finally, the various system properties and characteristics described in the body of the appendix are illustrated with several simple examples.

I. Introduction

State inequality constraints are commonly encountered in the study of dynamical systems. The study of rigid body aircraft dynamics and control is certainly no exception. For instance, a maximum allowable value of dynamic pressure is usually prescribed for aircraft with supersonic capability. This limit is required to ensure that the vehicle's structural integrity is maintained and constitutes an inequality constraint on vehicle state. State inequality constraints have been studied extensively by researchers in the field of optimal control, and necessary conditions for optimality when functions of state are constrained have been obtained[1-3]. However, the construction of solutions via this set of conditions proves very difficult, and most practitioners rely on direct

approaches to optimization that employ penalty functions for satisfaction of state inequality constraints[4].

As discussed in the literature, the use of singular perturbation techniques in the study of aircraft trajectory optimization can, through order reduction, lead to both open and closed loop solutions that are computationally efficient. These methods can also be used to circumvent difficulties associated with enforcing a state inequality constraint in the reduced solution[5]. As an example consider the minimum time intercept problem of[6]. A near optimal feedback solution is obtained via singular perturbation theory that includes consideration of an inequality constraint on dynamic pressure. In the zeroth-order reduced solution, algebraic constraints are obtained when the perturbation parameter, ε, which premultiplies the so called "fast" dynamic equations, is set to zero. These constraints can be used to eliminate the fast states (in this case altitude and flight path angle) from the reduced problem. One can choose, however, to retain one or more of the fast states and to eliminate instead some of the original control variables. The retained fast state variables are treated as new controls, and the original state constraint becomes a constraint involving both state and control in the reduced problem. In subsequent analysis of boundary layers, altitude resumes its status as a state variable, and dynamic pressure once again becomes a function of state alone. However, because the reduced solution for the example F-8 aircraft does not lie on the dynamic constraint boundary during ascent, the inequality constraint on dynamic pressure was not considered. Of note is the fact that modern supersonic fighter aircraft (such as the F-15) do ride the dynamic pressure constraint boundary during the ascent leg of the minimum time to intercept path.

In addition to the example cited above, dynamic pressure bounds are encountered during fuel-optimal climb for supersonic transports[7] for rocket powered launch vehicles such as the U.S. space shuttle[8] , and for single-stage-to-orbit air-breathing launch vehicles[9]. If, as in applying singular perturbation methods in seeking a solution to any of these problems, the reduced solution climb path lies directly on the dynamic pressure constraint boundary for a portion of the flight, then it is necessary to consider boundary layer transitions onto the constrained arc. This problem, which proves quite perplexing, has received almost no attention in the literature.

This appendix documents an initial investigation of the features of boundary layer transitions to state constrained arcs. Section II provides a brief review of first order necessary conditions derived for state-variable inequality constrained problems in optimal control. Section III discusses the optimal control of singularly perturbed systems subject to state-variable inequality constraints in general, and in particular examines the features of state inequality constrained boundary layers when the reduced solution lies on the constraint boundary. Section IV provides several simple

examples which illustrate the problem features discussed in earlier sections. Section V completes the appendix by providing some concluding remarks.

II. Constrained Problems in Optimal Control

The introduction of a state inequality constraint of the form

$$S(x,t) \leq 0 \tag{A.1}$$

can lead to considerable difficulty when attempting to obtain an optimal control solution. One approach to incorporating state inequality constraints into necessary conditions for optimality consists of constructing successive total time derivatives of S until explicit dependence on the control appears[11]. If p time derivatives are required then (1) is referred to as a p^{th} order state variable inequality constraint. The function $S^p(z,u,t)=0$ is then adjoined to the Hamiltonian as a constraint to be enforced when S=0. This approach introduces the following additional tangency conditions at the point of entry to a constrained arc

$$N(z,t) = \begin{bmatrix} S(z,t) \\ S^1(z,t) \\ \vdots \\ S^{p-1}(z,t) \end{bmatrix} = 0 \tag{A.2}$$

These same tangency conditions also apply at a point where the path leaves the constraint boundary. The equations (2) constitute a set of interior boundary conditions that must be met at each juncture between a constrained and unconstrained arc. Unfortunately, in order to satisfy these interior boundary conditions one must allow for the possibility of discontinuities in the costate variables at the junctures. An alternative set of necessary conditions can be obtained by adjoining the constraint function, rather than its p^{th} derivative, to the Hamiltonian and then employing a separating hyperplane theorem[22]. These conditions prove simpler and "sharper" than those of reference 11 however the possibility of discontinuous costates is still present. The gap between the necessary conditions of references 11 and 22 is defined in reference 23. A third alternative involves enploying a transformation technique in which a slack variable is used to transform the state inequality constrained problem into an unconstrained problem of higher dimension[30,31]. The work associated with the derivation of these first order necessary conditions is detailed in

references 32-38. Second order necessary conditions for optimality in the presence of state constraints have also been derived[39] as have conditions for various special cases[40]. Work continues in the area of state constrained optimization as evidenced by the approach of Lowen[41].

III. Optimization of Singularly Perturbed Systems Subject to State Inequality Constraints

Consider the system of singularly perturbed nonlinear differential equations:

$$dx/dt = f(x,y,u,t) \tag{A.3}$$

$$\varepsilon\, dy/dt = g(x,y,u,t) \tag{A.4}$$

with an index of performance of the form

$$J = \varphi[z(t_f), t_f] + \int_{t_o}^{t_f} L[z(t), u(t), t]dt \tag{A.5}$$

where x and f are of dimension n, y and g are of dimension m, $x(t_o)$ and $y(t_o)$ are given, ε is a small parameter, $t_o \le t \le t_f$, and the control u(t) is of dimension p. Zero order necessary conditions for optimality of the associated reduced and boundary layer problems in the absence of state constraints are readily available[42]. However, the following restrictions apply: f, g, $\partial f/\partial x$, $\partial f/\partial y$, $\partial g/\partial x$, and $\partial g/\partial y$ must be continuous and u must be piecewise continuous. Because of these restrictions on smoothness a direct extension of the necessary conditions of for state constrained problems to include singularly perturbed systems is not possible. This is due to the previously mentioned fact that discontinuities in the costates can occur at the junctures between constrained and unconstrained arcs. Alternately, the state inequality constrained singularly perturbed problem of interest can be converted into an unconstrained singularly perturbed problem of higher dimension by introduction of a slack variable[30]. This approach does eliminate the problem of discontinuous costates. However, the state constrained arc is replaced by a singular arc and the prospect of increased system dimension is unwelcome given the basic tenet of seeking order reduction.

Consider the flight dynamics problem detailed in the main body of this report. An inequality constraint on dynamic pressure of the form

$$S(h,V) = q - q_{max} \leq 0 \tag{A.6}$$

is to be enforced where

$$q = \rho V^2/2 \tag{A.7}$$

The symbol ρ represents atmospheric density and V represents the flight velocity. Given the equations of motion (1-4) expressed in the main body of this report, the first time derivative of (A.6) can be expressed as,

$$dS/dt = dq/dt = [V^3(\partial\rho/\partial r)/2 - \rho\mu V/r^2] \sin\gamma + \rho V(T - D)/m \tag{A.8}$$

Recall that the symbol T represents thrust, D, aerodynamic drag, m, vehicle mass, r, radial distance from the center of the Earth, γ, flight path angle, and μ, the gravitational constant for the Earth. Assume, as is typically done, that atmospheric drag can be represented as follows,

$$D = qsC_{Do} + KL^2/qs \tag{A.9}$$

where s represents an aerodynamic reference area, C_{Do},the zero lift drag coefficient, and K, the coefficient of the induced drag component. Note that the drag is explicitly dependent on the lift, L, which is treated as a control. In addition, the relation for thrust, T, is usually explicitly dependent on the engine throttle control. These controls appear explicitly in the first time derivative of the constraint function, (A.8), and it is thus classified as a first order state inequality constraint (i.e. p = 1). It is shown in reference 22 that when the constraint function is adjoined directly to the Hamiltonian and p = 1, no jumps in the costates will occur at the entry of an unconstrained arc onto a constrained arc. In this case the smoothness properties required by general singular perturbation theory are not violated and we may proceed with the application of singular perturbation methods with confidence.

The state inequality constraint on dynamic pressure is conveniently reduced to a state and control constraint function in construction of the reduced solution (i.e p becomes zero). This occurs because altitude, a state variable in the full order problem, becomes a control variable in the

reduced solution. Enforcing this state/control constraint in the reduced solution is a trivial matter. Now consider the construction of the zeroth order initial boundary layer. Assuming that energy is characterized as a slow state, application of the time stretching transformation $\tau = t/\varepsilon$ and again setting ε to zero yields an energy rate of zero. As such, the last term in (A.8) is no longer present. Instead, the first time derivative of the constraint function is given by,

$$dS/d\tau = dq/d\tau = [V^3(\partial\rho/\partial r)/2 - \rho\mu V/r^2] \sin\gamma \qquad (A.10)$$

With the last term of (A.8) absent, control dependence does not explicitly appear in (A.10). That is, the classification of the constraint function is altered following the time scale transformation when ε is set to zero. Taking the time τ derivative of (A.10), (i.e. forming the 2nd time τ derivative of S), yields a term containing the time derivative of the flight path angle, γ. The expression for flight path angle rate is as follows,

$$\gamma' = \frac{L}{mV} - \frac{\mu \cos\gamma}{Vr^2} + \frac{V \cos\gamma}{r} \qquad (A.11)$$

which is explicitly dependent on the lift control. Thus, in the boundary layer, the inequality constraint on dynamic pressure is 2nd order. Unfortunately, there is no guarantee that the costates are continuous for this case as there was for the case p = 1. Note that this type of behavior, in which the inequality constraint function order varies, is not present in all singularly perturbed problems with state inequality constraints, just for a certain class of them. For instance, if the constraint function is dependent on fast states alone, this variation does not occur.

If jumps in the costates are in fact present at the juncture between an unconstrained and a constrained arc, the smoothness properties required are violated and the available necessary conditions for optimal control of a singularly perturbed system cannot be applied directly. In some cases it is not possible for the boundary layer dynamic system to "ride" the constraint boundary before reaching the reduced solution. In such case the boundary layer costates can, at most, be discontinuous at the juncture between the initial boundary layer and the reduced solution and only if the reduced solution at that point is on the constraint boundary. It is also possible that no such jumps will occur.

If we proceed assuming that such jumps do not occur, then in most cases of interest the functional form of the boundary layer control solution in the presence of a state-variable inequality

constraint can be obtained. If this functional form involves an unknown costate, then use of the derived control solution is prevented unless the associated two point boundary value problem (TPBVP) is solved. To avoid solution of the TPBVP, as is desired in seeking a solution suitable for on-board, real-time implementation, an approximation for the unknown costate can be formed. If the costate history is continuous, the linearization technique of reference 43 can be applied to form the estimate. Unfortunately, for the case described above in which the reduced solution lies on the constraint boundary and the inequality constraint order is elevated to 2 by the boundary layer time scale transformation, purely imaginary roots result when the linearization technique is applied. Thus it is not possible to find a stablizing costate approximation given arbitrary initial states. In an unconstrained problem, the lack of an appropriate eigen-structure indicates that the problem does not exhibit the time scale properties assumed. Boundary layer transients do not exist for such cases; in fact there are fast oscillations that do not die out. The addition of an artificial cost term in formulation of the problem is suggested as an ad-hoc way to circumvent this difficulty. By proper choice of the weighting on can guarantee the proper structure of the linearized boundary layer system[44].

An interesting feature of the constrained boundary layer system described above is the presence of a finite costate rate at the juncture with the reduced solution. This behavior is illustrated in the sketch presented as Figure 1. In the figure, t_1 denotes the time at which an unconstrained arc joins a constrained arc (i.e. a juncture point).

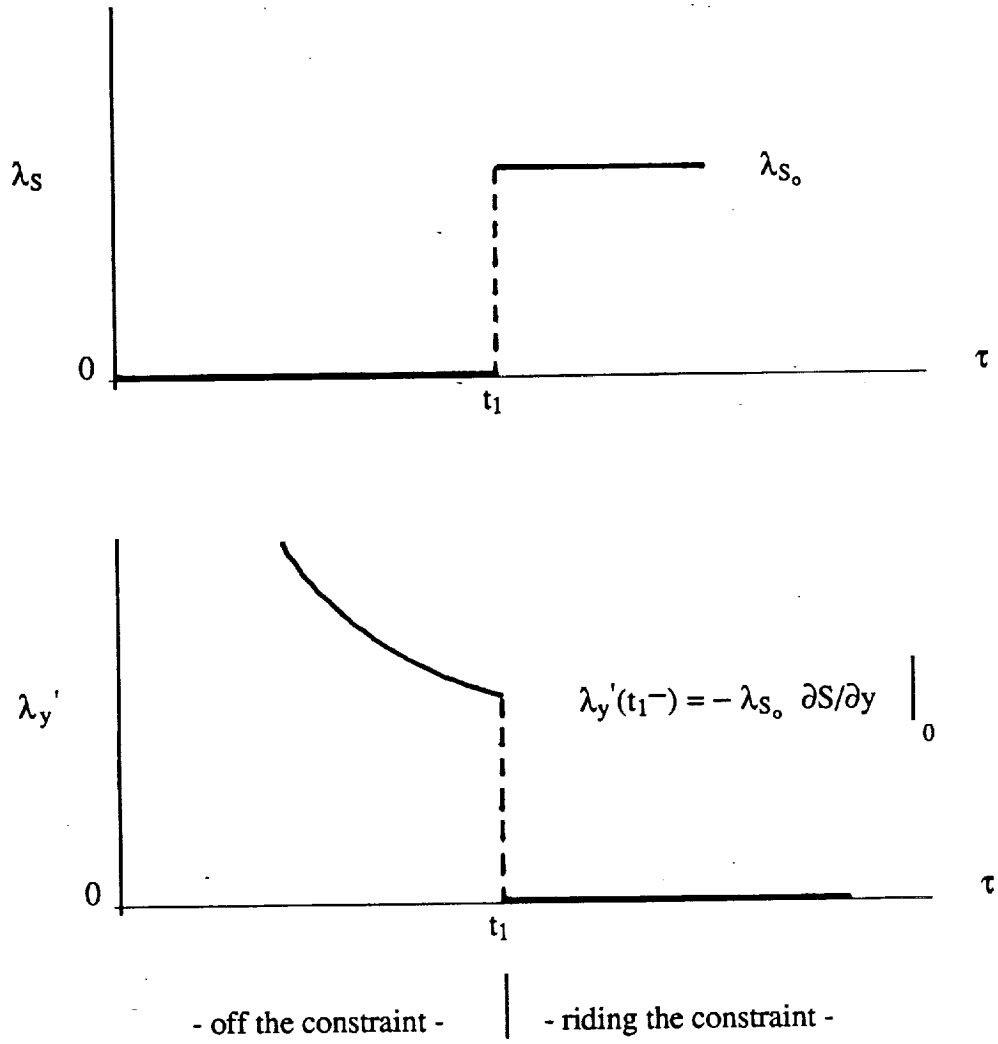

Figure 1 Illustration of finite costate rate at juncture between boundary layer and reduced solution trajectories.

Identification of the behavior illustrated in Figure 1 is based on the following construction.

$$\left.\frac{\partial H_{BL}}{\partial y}\right|_{\substack{u=u^* \\ S\le 0}} = \left.\frac{\partial H_{BL}}{\partial y}\right|_{\substack{u=\text{constant} \\ S\le 0}} + \cancelto{0}{\frac{\partial H_{BL}}{\partial u^*}}\frac{\partial u^*}{\partial y} \equiv -\lambda_y' \qquad \text{(A.12)}$$

Note that, since the last term in (A.12) is zero, this relation is equal to the negative of the costate rate. The following relation can also be constructed.

$$\left.\frac{\partial H_{BL}}{\partial y}\right|_{\substack{u=u^* \\ S\le 0}} = \left.\frac{\partial H_{BL}}{\partial y}\right|_{\substack{u=u^* \\ \text{unconstrained}}} + \lambda_S \frac{\partial S}{\partial y} \tag{A.13}$$

Now as τ tends to t_1^- we find that,

$$-\dot{\lambda}_y(t_1-) = \underbrace{\left.\frac{\partial H_{BL}}{\partial y}\right|_{\substack{u=\text{constant} \\ \text{unconstrained}}}}_{0} + \underbrace{\lambda_S \left.\frac{\partial S}{\partial y}\right|_{t_1^-}}_{0} \tag{A.14}$$

($\lambda_S = 0$ for $\tau < t_1$)

$$= -\lambda_{S_o} \left.\partial S/\partial y\right|_0 \quad \text{at } t_1^+ \text{ this becomes } \lambda_{S_o}$$

Thus the fast costate rate, $\dot{\lambda}_y$, has a finite value at t_1^- and then jumps to zero at t_1^+. The boundary layer system no longer approaches the reduced solution asymptotically as in the unconstrained case. Instead, a ***finite time*** boundary layer is implied. Similar finite time boundary layer phenomenon have been discovered by the investigators of interior boundary layers and boundary layers that approach singular arcs[45,46]. Using this terminal value for the costate rate it is possible to show analytically for problems of interest that the linearized boundary layer system will always have purely imaginary roots when the reduced solution lies on the state-variable inequality constraint boundary.

Consider the possibility of integrating the boundary system backwards in time from the reduced solution using the finite terminal value of costate rate to get started. Note that only a single extremal will be generated unless an additional free parameter is introduced into the problem. Since it should be possible to reach any set of initial conditions that do not violate the constraint, such a parameter surely exists. The only available parameter appears to be the magnitude of the possible costate jump at the juncture. This would imply that the costate history will be discontinuous at the juncture for all initial conditions that do not lie on the single extremal generated when it is assumed no jump occurs.

Assuming that first order necessary conditions for optimality can be obtained for which the requirement for smoothness can be relaxed (see for instance reference 47), one would again require a scheme for obtaining a stabilizing estimate of the unknown costates that appear in the optimal control law. However, to the author's knowledge, no directly applicable stability theory for finite time phenomenon is available for completing this task[48]. Alternately, one can consider transforming the constrained problem into an unconstrained problem, generally of higher order. The optimal trajectory of the transformed problem exhibits singular arcs which correspond, in the original constrained problem, to arcs which lie on the constraint boundary[30]. Because of this, the technique for costate approximation using the linearized boundary layer system, will fail. The reader is referred to the literature for a description of the work that has been done with regard to understanding control of singularly perturbed systems that include singular arcs[46].

IV. Examples

Several simple examples are now presented which illustrates the application of the Valentine transformation technique described in reference 46 *without* the penalty of increased system order[31]. The phenomena of a finite time boundary layer is illustrated in example 2.

Example 1

Consider the following singularly perturbed dynamical system with initial conditions at zero.

$$\dot{x}_1 = x_2 - u^2 \qquad x_1(0) = 0 \qquad \text{(A.15)}$$

$$\varepsilon \dot{x}_2 = x_3 \qquad x_2(0) = 0 \qquad \text{(A.16)}$$

$$\varepsilon \dot{x}_3 = u \qquad x_3(0) = 0 \qquad \text{(A.17)}$$

The following 2nd order (i.e. p = 2) state inequality constraint is to be enforced,

$$S = x_2 - 1 \leq 0 \qquad \text{(A.18)}$$

The final value of x_1 is specified, the final time is free, and the performance index is given by,

$$J = \int_0^{t_f} dt \tag{A.19}$$

Using Valentine's device, the inequality constraint (A.18) is converted into an equality by the introduction of a "slack variable," α^{30}.

$$S + \alpha^2/2 = 0 \tag{A.20}$$

Differentiating (A.18) p times (p = 2) with respect to time, the following set of equations is obtained,

$$x_3/\varepsilon + \alpha\alpha_1/\varepsilon = 0 \qquad \text{where } \varepsilon\, d\alpha/dt \equiv \alpha_1 \tag{A.21}$$

$$u/\varepsilon^2 + \alpha_1{}^2/\varepsilon^2 + \alpha\alpha_2/\varepsilon^2 = 0 \quad \text{where } \varepsilon\, d\alpha_1/dt \equiv \alpha_2 \tag{A.22}$$

Using the transformations $x_2 = 1 - \alpha^2/2$, $x_3 = \alpha\alpha_1$, and $u = -\alpha_1{}^2 - \alpha\alpha_2$, (A.15-17) become,

$$\dot{x}_1 = 1 - \frac{\alpha^2}{2} - \left(\alpha_1^2 + \alpha\alpha_2\right)^2 \tag{A.23}$$

$$\varepsilon\dot{\alpha} = \alpha_1 \tag{A.24}$$

$$\varepsilon\dot{\alpha}_1 = \alpha_2 \tag{A.25}$$

Reduced solution. By setting ε to zero, (A.24) and (A.25) are reduced to the following,

$$\overset{o}{\alpha}_1 = 0 \tag{A.26}$$

$$\overset{o}{\alpha}_2 = 0 \tag{A.27}$$

The reduced solution Hamiltonian is given by,

$$H = \lambda_x \left[1 - \frac{\alpha^2}{2} - \left(\alpha_1^2 + \alpha\alpha_2 \right)^2 \right] + \lambda_\alpha \alpha_1 + \lambda_{\alpha_1} \alpha_2 + 1 = 0 \qquad \text{(A.28)}$$

Evaluation of first order necessary conditions for optimality results in the following,

$$H = 0 \;\; \& \;\; H_\alpha = 0 \quad \Rightarrow \quad \lambda_x^o = -1 \,, \quad \alpha^o = 0 \qquad \text{(A.29)}$$

$$H_{\alpha_1} = 0 \quad \Rightarrow \quad \lambda_\alpha^o = -1 \qquad \text{(A.30)}$$

$$H_{\alpha_2} = 0 \quad \Rightarrow \quad \lambda_{\alpha_1}^o = -1 \qquad \text{(A.31)}$$

Boundary Layer Problem. Introducing the time scale transformation $\tau = t/\varepsilon$ and again setting ε to zero, the boundary layer dynamics are given by

$$\alpha' = \alpha_1 \qquad \text{(A.32)}$$

$$\alpha_1' = \alpha_2 \qquad \text{(A.33)}$$

where the prime notation denotes differentiation with respect to the stretched time τ. The boundary layer Hamiltonian is given by,

$$H_{BL} = \frac{\alpha^2}{2} + \left(\alpha_1^2 + \alpha\alpha_2 \right)^2 + \lambda_\alpha \alpha_1 + \lambda_{\alpha_1} \alpha_2 = 0 \qquad \text{(A.34)}$$

The costate dynamics are given by

$$\lambda_\alpha' = -\alpha - 2\left(\alpha_1^2 + \alpha\alpha_2 \right)\alpha_2 \qquad \text{(A.35)}$$

$$\dot{\lambda}_{\alpha_1} = -4\left(\alpha_1^2 + \alpha\alpha_2\right)\alpha_1 - \lambda_\alpha \tag{A.36}$$

And when the constraint is inactive, the control, α_2, is determined by the necessary condition,

$$\frac{\partial H_{BL}}{\partial \alpha_2} = 2\left(\alpha_1^2 + \alpha\alpha_2\right)^2\alpha + \lambda_{\alpha_1} = 0 \tag{A.37}$$

Note that when the constraint is active, α is zero and the condition (A.37) yields no direct control solution. Riding the constraint boundary corresponds to a singular arc in the transformed problem.

Example 2

Consider a simplification of Example 1, namely the singularly perturbed dynamical system,

$$\dot{x}_1 = x_2 - u^2 \tag{A.38}$$

$$\varepsilon \dot{x}_2 = u \tag{A.39}$$

The inequality constraint (A.18) becomes a 1st order (i.e. p = 1) state inequality constraint,

$$S = x_2 - 1 \leq 0 \tag{A.40}$$

The final value of x_1 is again specified, the final time is free, and the performance index is again given by,

$$J = \int_0^{t_f} dt \tag{A.41}$$

Using Valentine's device, the inequality constraint (A.40) is converted into an equality by the introduction of a "slack variable," α[30].

$$S + \alpha^2/2 = 0 \tag{A.42}$$

Differentiating (A.42) p times (p = 1) with respect to time, the following equation is obtained,

$$u/\varepsilon + \alpha\alpha_1/\varepsilon = 0 \qquad \text{where } \varepsilon\, d\alpha/dt \equiv \alpha_1 \tag{A.43}$$

Using the transformations $x_2 = 1 - \alpha^2/2$ and $u = -\alpha\alpha_1$, (A.38-39) become,

$$\dot{x}_1 = 1 - \frac{\alpha^2}{2} - (\alpha\alpha_1)^2 \tag{A.44}$$

$$\varepsilon\dot{\alpha} = \alpha_1 \tag{A.45}$$

Reduced solution. By setting ε to zero, (A.45) is reduced to the following,

$$\alpha_1^o = 0 \tag{A.46}$$

The reduced solution Hamiltonian is given by,

$$H = \lambda_{x_1}\left[1 - \frac{\alpha^2}{2} - (\alpha\alpha_1)^2\right] + \lambda_\alpha\alpha_1 + 1 = 0 \tag{A.47}$$

Evaluation of first order necessary conditions for optimality results in the following,

$$H = 0 \;\; \& \;\; H_\alpha = 0 \quad \Rightarrow \quad \lambda_x^o = -1, \quad \alpha^o = 0 \tag{A.48}$$

$$H_{\alpha_2} = 0 \quad \Rightarrow \quad \lambda_\alpha^o = 0 \tag{A.49}$$

from which it is evident that

$$x_1^o(t) = t \tag{A.50}$$

$$x_2^o(t) = 1 \tag{A.51}$$

Boundary Layer Problem. Introducing the time scale transformation $\tau = t/\varepsilon$ and again setting ε to zero, the boundary layer dynamics are given by

$$\alpha' = \alpha_1 \tag{A.52}$$

where the prime notation denotes differentiation with respect to the stretched time τ. The boundary layer Hamiltonian is given by,

$$H_{BL} = \frac{\alpha^2}{2} + (\alpha\alpha_1)^2 + \lambda_\alpha \alpha_1 = 0 \tag{A.53}$$

The costate dynamics are given by

$$\lambda_\alpha' = -\alpha\left(1 + 2\alpha_1^2\right) \tag{A.54}$$

The condition that the partial derivative of the Hamiltonian with respect to the control be zero yields the following result,

$$H_{\alpha_1} = 0 \quad \Rightarrow \quad \alpha_1 = -\frac{\lambda_\alpha}{2\alpha^2} \tag{A.55}$$

Substituting this result back into the condition that the Hamiltonian be zero, the following result is obtained.

$$H = 0 \quad \Rightarrow \quad \lambda_\alpha = \pm\sqrt{2}\,\alpha^2 \tag{A.56}$$

Substituting (64) into (63) we find that the optimal value of the control, α_1, is constant; namely,

$$\alpha_1^* = \pm\frac{1}{\sqrt{2}} \tag{A.57}$$

With this result it is possible to integrate equation (A.52) to obtain,

$$\alpha(\tau) = \sqrt{2} \pm \frac{\tau}{\sqrt{2}} \tag{A.58}$$

When the boundary layer trajectory reaches the constraint boundary (i.e. $x_2 = 1$), $\alpha = 0$ and the expression (A.58) yields a finite final time of 2 units of boundary layer time. Transforming back, we obtain an expression for u in terms of x_2,

$$u^* = \sqrt{1 - x_2} \tag{A.59}$$

where integration of the original differential equation (A.39) yields,

$$x_2 = 1 - \left(1 - \frac{\tau}{2}\right)^2 \tag{A.58}$$

V. Conclusions

In conclusion, state-variable inequality constrained singularly perturbed problems can exhibit complex boundary layer phenomenon that are not well understood. The order of the state constraint can increase when going from the full order problem to a boundary layer analysis. Because discontinuous costate histories can be introduced by the presence of state inequality constraints, a direct application of available singular perturbation theory, which requires the state and costate histories to be smooth, is not possible. The boundary layer phenomenon associated with such problems appear to be finite time. A stability theory for finite time phenomenon, as required to construct a suitable approximation for costates appearing in derived feedback control laws, is not available at this time. Valentine's transformation can be used to overcome some of these difficulties, but at the expense of introducing singular arcs and possibly increased system order.

Appendix B

Permormance Modeling of Hypersonic Vehicles

I. Introduction

In order to carry out useful performance studies, trajectory optimization and guidance law development for hypersonic transatmospheric vehicles, it is necessary to utilize an accurate model of the aerodynamics and propulsion system characteristics. Since actual vehicle design is not involved, it is appropriate to utilize simplified models if they can be made to properly reflect the actual vehicle performance characteristics. It is also of great benefit to have available models that can be used interactively to study the impact of small changes in vehicle configuration or propulsion system design.

In what follows is described a set of simple algorithms devised for use in the present research program for the purposes outlined. The computer codes have evolved continuously throughout the study. The result is an integrated hypersonic vehicle performance package that has many applications beyond those originally envisioned.

II. Hypersonic Aerodynamic Performance Modeling

Simple hypersonic aerodynamic theory enables construction of practical and highly accurate representations of the performance characteristics of realistic hypersonic flight vehicles. In this section we review the basic theoretical approach and the implementation of this theory in the form of interactive computer software. The basic approach was to make the application of the model to a particular airframe conceptual design as simple as possible. Because of the interactive nature of the algorithms used, effects of even minor design modifications can be immediately assessed in terms of sensitivity parameters such as L/D ratio, overall vehicle drag coefficient, and trim moments.

The models developed have applications that range considerably beyond the ones addressed in this report. For example, they are a sufficiently accurate representation of the vehicle performance to allow assessment of off-design flight conditions as well as approximate stability and control studies. Although the emphasis in the following discussion is on the high-Mach number performance modeling, the computer program under development is being set up to cover the entire Mach number range from low subsonic to hypersonic speeds. The low speed aerodynamic performance models used are not as accurate as those in the hypersonic

range, but are sufficiently precise for use in simple performance modeling in which low speed flight affects such as the landing or takeoff flight phases are to be included.

In what follows is given a brief description of the operation of the computer program and the basic theory on which it is based. The methods used in applying the theory to a given vehicle configuration is reviewed for the benefit of readers unfamiliar with hypersonic aerodynamic modeling.

User Interface

The computer algorithms were designed to make their application to a given vehicle configuration as simple as possible. At present, limited access to actual flight vehicle configurations makes it necessary to work from rather sparse data sets. For example, the vehicle to be studied may be defined only by a simple three-view drawing. We have deliberately set out to make it possible to work effectively from such data. The configuration is entered into the program in a variety of ways. The simplest method allows input in the form of outlines of the wing planform, fuselage elevation and planform, body cross-section shapes, and tail surface configuration in the form of discrete points. It is not necessary that a large number of outline points be used. For example fuselage outline data can consist of as few as ten points in elevation and planform with acceptable accuracy. The program allows for variation in fuselage cross-section station by station along the axis of symmetry. It also allows for corners in the cross-section as often chosen in hypersonic vehicle layouts.

The configuration data can also be entered by scanning a three-view of the vehicle. Scaling is accomplished by selecting points at the nose and tail of the planform. The user then selects points interactively by means of a mouse or graphics table. Modifications in geometry can be directly implemented in the input process by altering position of control points. Wing and tail incidence, fin cant, control surface deflection , and other required information are entered in an interactive tabular input window. If insufficient data has been entered to properly define the complete configuration, the program warns the operator and indicates what additional information must be specified.

Interactive Program Mode

The computer program has been designed to take full advantage of modern computer graphical interface technology. Once a vehicle configuration has been implemented as described earlier, its attributes can be saved and modified later. At the discretion of the user, one or more attributes of the vehicle aerodynamic performance characteristics can be displayed simultaneously with the configuration input panel. For example, the lift coefficient vs angle of attack, lift/drag ratio, pitching moment vs lift coefficient or other information can be viewed at the same time changes in vehicle geometry such as wing area, incidence angle, airfoil shape, or

body cross-section shape are being input. This makes it very easy to determine the impact of design changes in a direct and graphically useful manner. When the program is linked to one of the postprocessing packages such as the one describing trajectory optimization discussed elsewhere in the report, it is possible to view effects of configuration modifications directly in terms of their impact on selected performance parameters.

Local Surface Inclination Theory with Blast Wave Corrections

Several decades of experience have shown that the simplest form of hypersonic flow field modeling yields a practical and accurate means for estimating vehicle performance. The Newtonian flow model gives an excellent representation for the pressure changes on the vehicle surfaces directly in terms of the inclination of the local surface to the freestream flow. Various modifications can also be applied to correct the pressure distribution for effects of strong shock formations at the leading edges of lifting surfaces and tail surfaces and on the nose of thefuselage. The blast wave theory is employed for this purpose.

Simple Newtonian impact theory shows that the pressure coefficient at any point on the windward vehicle surface is given by

$$C_p = 2\sin^2\theta \tag{B.1}$$

Thus all that is necessary to apply it to a three dimensional vehicle is to set up an algorithm that utilizes geometry information to determine whether a given element of the surface is on the windward side and to calculate the angle between the freestream velocity vector and the surface element. Samples of the computational method used in this program are discussed briefly in the following subsections.

Hypersonic Thin Airfoil Theory

In some situations, it is sufficiently accurate to represent hypersonic lifting surfaces as flat plates. However, in practical situations the need for adequate low-speed aerodynamic characteristics and surface structure dictates that a cambered airfoil of reasonable thickness be used. For example, the NASA vehicle designs used in our computations typically employed airfoils of of between 5 and 10% maximum thickness ratio. Thus it is useful to provide means for correcting the force calculations for camber and thickness effects. Figure B.1 defines the required geometry for a typical wing section.

On the windward side of the airfoil, the camber/thickness function is conveniently described as a functional relationship

$$y_\ell = F(x) \tag{B.2}$$

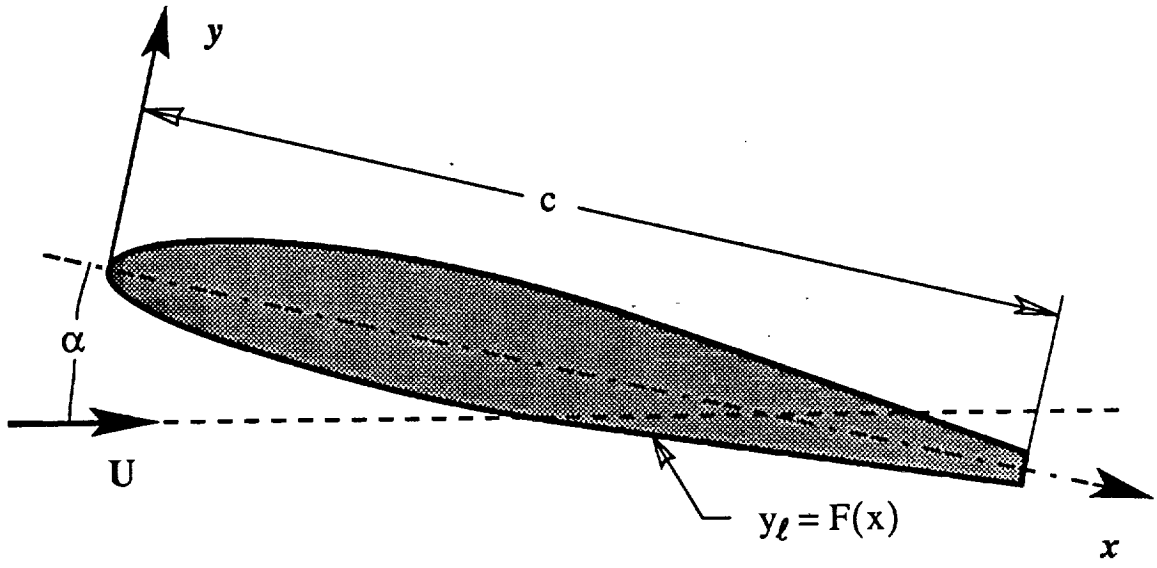

Figure B.1. Hypersonic Airfoil

This can be input in the computer program as a series of points taken from a scan of the airfoil or by inputing in tabular form. The program also allows the specification of the airfoil profile directly in analytical form. The program logic then determines the required calculation module from which to compute the wing characteristics. The program also contains provision for accounting for wing twist, although none of the vehicle models studied have employed twist. The local value of the pressure coefficient becomes

$$C_p = 2\sin^2\left(\alpha + \iota - \frac{dF}{dx}\right) \tag{B.3}$$

where α is the vehicle angle of attack measured between the fuselage reference plane (See Figure B.2), ι is the incidence angle between the wing chord line and the fuselage reference plane, and F is the airfoil envelope shape function as described above. This information is then used as the basis for determining the normal force coefficient for the airfoil. The result is

$$c_n = \frac{2}{c}\int_0^c \sin^2\left(\alpha + \iota - \frac{dF}{dx}\right) dx \tag{B.4}$$

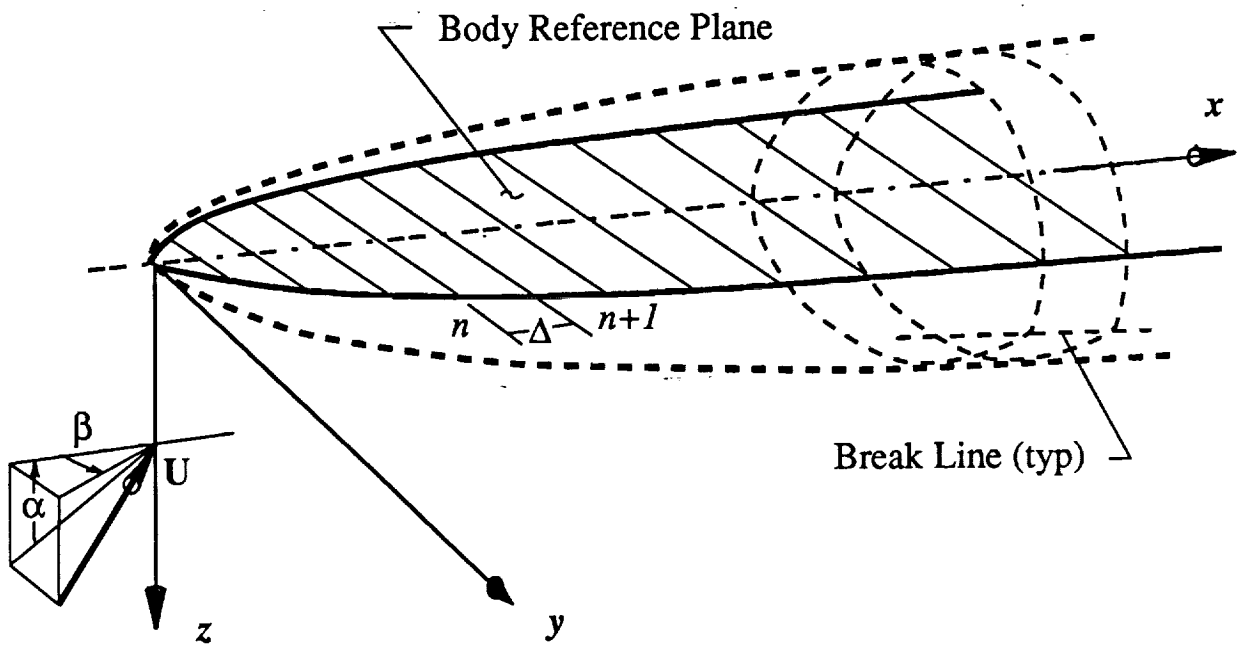

Figure B.2. Definition of Fuselage Reference Plane

and from this we find the section lift and drag coefficients.

$$\begin{cases} c_\ell = \dfrac{2\cos\alpha}{c}\displaystyle\int_0^c \sin^2\left(\alpha + \iota - \frac{dF}{dx}\right) dx & \text{(B.5)} \\ c_d = \dfrac{2\sin\alpha}{c}\displaystyle\int_0^c \sin^2\left(\alpha + \iota - \frac{dF}{dx}\right) dx & \text{(B.6)} \end{cases}$$

These coefficients are then used with the wing planform information giving the local values of chord length and incidence (for a twisted wing) to determine the force on the local wing section. The results for the entire wing are then accumulated. The program has provision for displaying the total lift and drag coefficients and the center of pressure location for the three-dimensional wing. It also determines contributions to the pitch, yaw, and roll moment coefficients.

Aileron, elevon or flaperon deflection effects are also computed. The user must input the desired control surface deflections. Differential elevon deflections are allowed. The program senses when the critical surface deflection angle (at which the freestream flow no longer impinges on the deflected surface) has been exceeded and properly adjusts the force system.

Hypersonic Lifting Body Theory

The integrated fuselage/propulsion system provides most of the lift of a typical hypersonic aircraft. Since the shapes may be somewhat complex, it is necessary to provide for an adequate geometrical representation. Figure B.2 shows the coordinate system used and defines the vehicle reference plane. This plane typically coincides with the body centerline as seen in the elevation drawing, but the program allows for arbitrary specification of this plane. For convenience, the origin of the coordinate system is located at the vehicle nose. The x-axis lies along the reference plane in the (assumed) normal plane of symmetry. The y-axis points to the left and the z-axis points downward.

Figure B.3 shows how the various profile curves defining the body shape are represented in the program. These curves may be determined by curve fitting of three-view drawings or may be input into the program as a table of points. It is not necessary to utilize a large number of points. Ten points per profile curve usually provide adequate accuracy unless the body shapes are exceptionally complex.

As shown in Figure B.3, the body cross-section profiles are not required to be continuous curves. Corners are allowed as represented by the break points shown in the drawings. The fuselage shape is specified in functional form as

$$\begin{cases} z = f(y) & \text{Cross Section Shape} \\ y = g(x) & \text{Planform Shape} \\ z = h(x) & \text{Fuselage Elevation} \end{cases} \tag{B.7}$$

These functions are determined in the program from the input coordinate points and are used to compute the unit vector normal to a point on the windward surface. The result is

$$\mathbf{n} = \sin\phi_1 \mathbf{i} + \sin\phi_2 \mathbf{j} + (\cos\phi_1 \cos\phi_2)\mathbf{k} \tag{B.8}$$

where

$$\phi_1 = \tan^{-1}\left(\frac{dh}{dx}\right) \tag{B.9}$$

$$\phi_2 = \tan^{-1}\left(\frac{df}{dy}\right) \tag{B.10}$$

An area element of the body surface at the same location can be written as

$$dS = \frac{\Delta}{\cos\phi_1 \cos\phi_2} dy \tag{B.11}$$

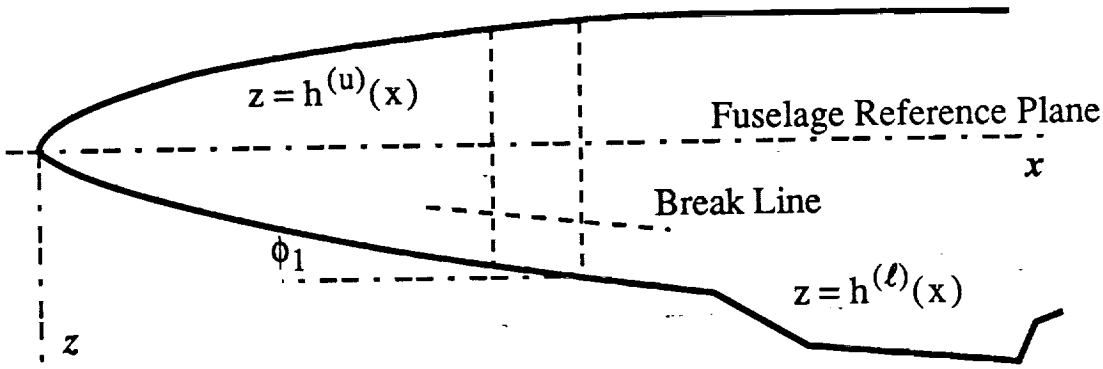

Fuselage Elevation

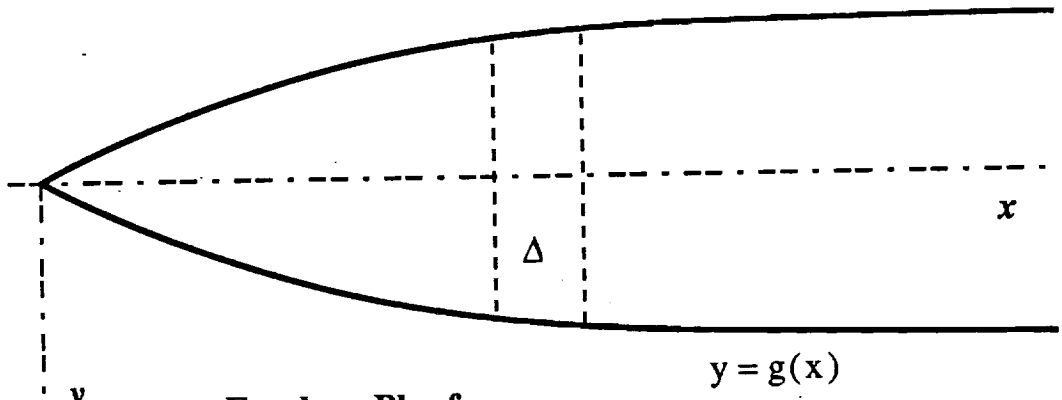

Fuselage Planform

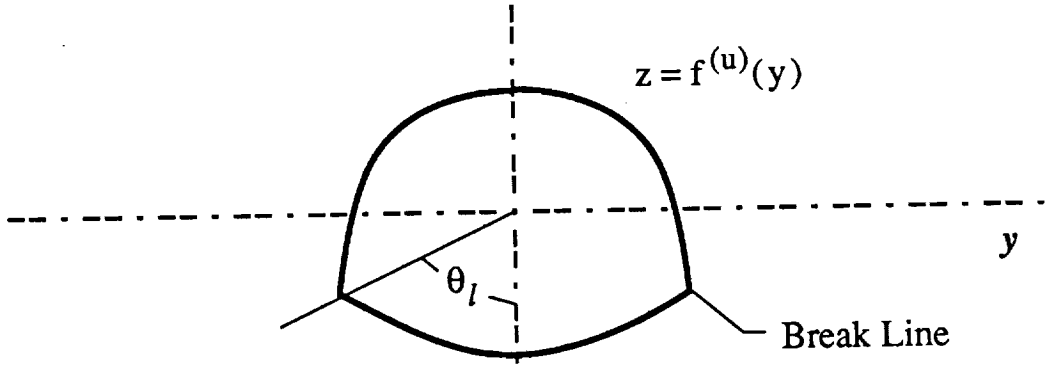

Cross-Section

Figure B.3. Definition of Body Shape Functions

The projected width of the element in the reference plane is Δ as shown in Figure B.3. The inclination angle between the freestream velocity vector and the surface element is given by

$$\psi = \cos^{-1}\left(\frac{\mathbf{U}_\infty \cdot \mathbf{n}}{U_\infty}\right) - \frac{\pi}{2} \tag{B.12}$$

where the velocity vector is specified in body coordinates as

$$\mathbf{U}_\infty = U_\infty[(\cos\beta\cos\alpha)\mathbf{i} - (\sin\beta)\mathbf{j} - (\cos\beta\sin\alpha)\mathbf{k}] \tag{B.13}$$

The local pressure coefficient is

$$C_p = 2\sin^2[\psi] \tag{B.14}$$

The dimensionless normal force vector on the surface element is, in vector form

$$d\mathbf{F} = -2\sin^2[\psi]\, dS\, \mathbf{n} \tag{B.15}$$

Integration of this function across the width of the body gives the force vector on an axial element of the vehicle. The program then sums all contributions axially to determine the lift, drag, sideforce, and moment coefficients for the complete assembly.

The more detailed representation of the body geometry used in the present version of the program greatly improves the agreement between the predicted and measured aerodynamic performance. Earlier problems with the vehicle lift curve slope at zero angle of attack have been eliminated because the effects of body curvature and surface orientation are now properly accommodated in the calculations.

III. Scramjet Propulsion Model

Although the supersonic combustion ramjet concept has been known for over two decades, the lack of appropriate unclassified experimental data, cycle analyses, and combustion analyses requires that we use a simple conceptual model for the purposes of vehicle trajectory optimization. In what follows is a brief description of this model and the philosophy behind it.

Conceptually, the SCRAMJET is as simple an airbreathing combustion device as one could imagine. In the case of the new family of flight vehicles to use this propulsion concept,

the entire underside of the vehicle plays a role in the operation of the system. Figure 1 shows the basic configuration. Mechanically, the device can be thought of in terms of three elements. These are

1. Diffuser
2. Combustor
3. Expansion nozzle

Hypersonic vehicle designers attempt to utilize the forward fuselage, strakes, and wings to provide the majority of the diffusion. The lower part of the three-dimensional oblique shock formed at the leading edges is tailored to the shape of the combustor inlet so that air enters at approximately a Mach number of the order of 3 depending on the flight speed. Combustion of hydrogen fuel takes place in the duct at supersonic speeds in order to minimize energy losses due to dissociation, which would be enormous if the more conventional subsonic ramjet cycle were to be used in high speed flight. Liquid hydrogen is the fuel of choice not only because of its high energy content, but because it can be made to burn in a supersonic flow due to its wide flammability limits and high flame speed. Finally, the combustion products are expanded through a nozzle, which, like the diffuser is designed into the contour of the lower fuselage.

The propulsion system is mostly diffuser and nozzle. While these elements are fairly easy to model from the thermodynamic cycle point of view, the aerodynamics are quite complex, giving rise to a challenging design problem. Computational fluid dynamics (CFD) numerical techniques are being relied upon in conjunction with a new family of hypersonic test facilities to yield practical design solutions. Unfortunately, information on the current research is classified, so that realistic design data is not available for projects of the type reported here.

The computational model used here to represent the SCRAMJET propulsion system was deliberately designed to be readily updated as new information becomes available. It directly accesses a standard atmosphere model (also easily adjustable to provide non-standard operating conditions), which simplifies its incorporation into a trajectory optimization program. The diffuser and nozzle performance is determined either with standard thermodynamic models or by means of optimal design curve fits such as those proposed by Billig. Since information concerning recent progress in supersonic combustion was not available, a simple combustor model was incorporated. This is a straightforward Rayleigh line calculation. An iterative scheme is used to determine the nozzle entrance Mach number, by maintaining the mixture ratio at or below the stoichiometric value. No detailed combustion calculations with multi-species gases is attempted in the present version of the model although these could be readily incorporated as a more definitive model of practical SCRAMJET combustion comes into focus.

The propulsive drag estimate of Billig was incorporated to account in a simple way for some of the frictional losses. No attempt was made to incorporate vehicle integration effects in an interactive fashion. Experience with the aerodynamic simulation shows that very small vehicle attitude changes take place during equilibrium flight. Therefore in the present state of development, no vehicle attitude dependence has been included in the propulsion model. The flexibility of the algorithm will make such additions quite easy to incorporate as the need for them is established.

References

B.1. Billig, F. S., "Design Considerations of Supersonic Combustion Ramjets," AIAA-86-0159, AIAA 24th Aerospace Science Meeting, Jan 6-9, 1986.

B.2. Northam, G. B. and G. Y. Anderson, "Supersonic Combustion Ramjet Research at Langley," AIAA-86-0159, AIAA 24th Aerospace Science Meeting, Jan 6-9, 1986.

B.3. Avery, W. H. and Dugger, G. L., "Hypersonic Airbreathing Propulsion," Astronautics and Space Engineering, June 1964, pp 42-47.